

Spatio-Temporal Stochastic Pattern Generator for ensemble prediction and ensemble data assimilation in geophysical applications

Michael Tsyrulnikov and Dmitry Gayfulin

HydroMetCenter of Russia

(mik.tsyrulnikov@gmail.com)

December 3, 2024

Abstract

A generator of spatio-temporal pseudo-random Gaussian fields that satisfy the “proportionality of scales” property (Tsyroulnikov 2001) is presented. The generator is a third-order in time stochastic differential equation with a pseudo-differential spatial operator defined on a limited area domain in Cartesian coordinate system. The spatial covariance functions of the generated fields belong to the Matérn class. The spatio-temporal covariances are non-separable. A spectral-space numerical solver is implemented and accelerated exploiting properties of real-world geophysical fields, in particular, smoothness of their spatial spectra. The generator is designed to simulate additive or multiplicative, or other spatio-temporal perturbations that represent uncertainties in numerical prediction models in geophysics. The program code of the generator is publicly available.

Contents

1	Introduction	3
2	SPG: Requirements	5
3	The proposed solution	6
4	Tentative first-order evolutionary model for SPG	7
4.1	Solution of the SPG model equation in spectral space	7
4.2	Stationary space-time covariance functions	8
4.2.1	Spectral-space statistics	8

4.2.2	Physical-space statistics	9
4.2.3	Spatial isotropy	10
4.3	“Proportionality of scales” implies that $q = \frac{1}{2}$	10
4.4	Admissible spatial spectra	11
4.4.1	Spatial covariance functions	11
4.4.2	Finite variance requirement	12
4.4.3	Implications for the SPG design	12
5	Higher-order in time model	13
5.1	Formulation	13
5.2	Stationary spectral-space statistics	13
5.3	Finite-variance criterion	14
6	Spatio-temporal covariances for the higher-order in time SPG model	14
6.1	Spatial correlation functions: the Matérn class	14
6.2	Temporal correlation functions	16
6.3	Spatio-temporal correlations	17
7	The final formulation of the SPG model	18
8	Time discrete solver for the third-order in time SPG model	19
8.1	The spectral solver	19
8.2	Correction of spectral variances	20
8.3	“Warm start”: ensuring stationarity from the beginning of time integration	20
8.4	Computational efficiency	21
8.4.1	Making the time step Δt dependent on the spatial wavenumber k .	21
8.4.2	Introduction of a coarse grid in spectral space	21
8.4.3	Numerical acceleration: results	22
8.5	Examples of the SPG fields	24
9	Discussion	24
9.1	Physical-space or spectral-space SPG solver?	24
9.2	Extensions of the SPG	25
10	Conclusions	26
10.1	SPG: summary	26
10.2	Applications	27
Acknowledgements		27
Appendices		27
A Illustration of the “proportionality of scales” property		27

B Spatio-temporal structure of the driving 4-D noise	28
B.1 White noise	28
B.2 Space-integrated spatio-temporal white noise on $\mathbb{T}^d \times \mathbb{R}$	28
B.3 Spatial spectrum of a spatio-temporal white noise	30
B.4 Spectral decomposition of a white in time and colored in space noise	31
B.5 Discretization of the spectral processes $\tilde{\alpha}_{\mathbf{k}}(t)$ in time	31
C Physical-space approximation of the operator $\sqrt{1 - \lambda^2 \Delta}$	32
D Stationary statistics of a higher-order OSDE	34
E Smoothness of sample paths of the spatial Matérn random field for different ν	35
F Stationary statistics of a time discrete higher-order OSDE	36
F.1 First-order numerical scheme	36
F.2 Third-order numerical scheme	36
Bibliography	38

1 Introduction

Any model of a natural system is imperfect. To account for the inevitable uncertainty of the model, the general approach called *stochastic dynamic modeling* is used. According to this paradigm, the physical (often also called dynamical) model of the system is appended with a stochastic model of *model errors*. The output (e.g. prediction) of the physical model then becomes a probability distribution.

The aim of the introduction of the stochastic component is twofold. First, the output probability distribution provides a (valuable) measure of the *uncertainty* in the physical model's prediction, leading to probabilistic forecasting. Second, for a nonlinear physical model, switching from a deterministic prediction to the expected (mean) value of the output probability distribution improves the mean-square accuracy of the prediction, i.e. improves the deterministic forecasting.

Application of the stochastic dynamic paradigm to complex geophysical systems is, however, hampered by their high dimensionality and non-linearity. The output probability distribution appears to be neither analytically nor numerically tractable. An affordable approximate solution is provided by the Monte-Carlo method called in geophysics *ensemble modeling*.

In ensemble modeling, the model uncertainty is represented by *pseudo-random draws* from the model-error probability distribution rather than by the distribution itself. A relatively small affordable number of these draws are fed to the model giving rise to an

ensemble of predictions. If the simulated model errors are drawn from the correct model-error distribution (and all other sources of uncertainty are correctly sampled as well), then the members of the resulting ensemble of predictions appear to be draws from the correct probability distribution of the truth given the available initial and boundary conditions for the physical model. This mathematically justifies the ensemble modeling principle. From the practical perspective, members of the prediction ensemble can be interpreted as “potential truths” consistent with all available information.

Meteorological ensemble prediction and ensemble data assimilation follow this general ensemble modeling paradigm. In particular, errors due to imperfect forecast-model equations and imperfect formulations of boundary conditions (called model errors) need to be adequately sampled. But justified stochastic model-error models are still to be devised and verified. In the authors’ opinion, the best way to stochastically represent spatio-temporal forecast-model-error fields is to treat each error source separately, so that, say, each physical parametrization is accompanied with a spatio-temporal stochastic model of its uncertainty. Or, even better, to completely switch from deterministic physical parameterizations to stochastic ones. There is a growing number of such developments (see Berner et al., 2015, for a review), but the problem is so complex that we cannot expect it to be solved in the near future. Its solution is further hampered by the fact that the existing meteorological observations are too scarce and too inaccurate for model errors to be objectively identified by comparison with measurement data with satisfactory accuracy (Tsyrulnikov and Gorin, 2013).

As a result, in meteorology ad-hoc model-error models are widely in use. The existing approaches include generating pseudo-random additive or multiplicative perturbations of the right-hand sides of the model equations (e.g. Houtekamer et al., 2009; Buizza et al., 1999) in the course of forecast. These two model-error modeling techniques as well as Stochastic Kinetic Energy Backscatter schemes (Berner et al., 2009) require a pseudo-random spatio-temporal field as a stochastic input. Stochastic parameterization schemes can also demand such fields (see e.g. Bengtsson et al., 2013), whose generation is the subject of the present report.

The simplest pseudo-random field is, obviously, the white noise, i.e. the uncorrelated in space and time random field. The white noise is the default forcing in stochastic differential equations (e.g. Jazwinski (1970) or Arnold (1974)). Its advantage is the complete absence of any spatio-temporal structure, it is a pristine source of stochasticity. But in model-error modeling, this lack of structure precludes its direct use either as an additive or multiplicative perturbation field because model errors are related to the weather pattern and so should be correlated (dependent) both in space and time. Tsyrulnikov (2005) showed in a simulation study that model errors may exhibit complicated spatio-temporal behavior.

The simplest way to obtain a correlated pseudo-random spatio-temporal field is to compute an independent random number at each point of a *coarse* spatio-temporal grid and then assign it to all model grid grid point within the coarse-grid cell (Buizza et al.,

1999). As a result, the model-grid field becomes correlated in space and time. The decorrelation space and time scales are, obviously, defined by the respective coarse-grid spacings. This determines the choice of the coarse grid, e.g. in (Buizza et al., 1999) the spatial grid spacing was about 1000 km and the temporal one 6 hours). This technique is extremely simple but it suffers from two flaws.

First, the resulting interpolated model-grid field appears to be discontinuous and inhomogeneous. Second, the spatio-temporal structure of the field is not scale dependent, that is, the resulting temporal length scales do not depend on the respective spatial scales. In reality, longer spatial scales ‘live longer’ than shorter spatial scales, which ‘die out’ quicker. This ‘proportionality of scales’ is widespread in geophysical fields (see Tsyrounikov, 2001, and references therein) and other media, (see e.g. Meunier and Zhao, 2009, p.129), so we believe it should be represented by model-error models. Note also that “proportionality of scales” is a special case of *non-separability* of spatio-temporal covariances. For a critique of simplistic separable space-time covariance models, see (Cressie and Huang, 1999; Stein, 2005; Gneiting et al., 2006) and Appendix A in this report.

Another pseudo-random field generation technique in space and time employs a spectral transform in space and then imposes independent temporal auto-regressions for the coefficients of the spectral expansion (Li et al., 2008; Berner et al., 2009; Bowler et al., 2009; Palmer et al., 2009; Bouttier et al., 2012). This technique is more general and produces homogeneous fields, but the above implementations use *the same time scale* for all spatial wavenumbers so that there are still no space-time interactions in the generated spatio-temporal fields.

In this report, we propose and test a spatio-temporal Stochastic (pseudo-random) Pattern Generator (SPG) that accounts for the above ‘proportionality of scales’ and imposes meaningful space-time interactions. The SPG operates on a limited-area domain. It is based on a (spectral-space) solution to a stochastic partial differential equation, more precisely, on a stochastic differential equation in time with a pseudo-differential spatial operator. In what follows, we present the technique, describe its numerical approximation, and examine properties of the resulting generated spatio-temporal fields in 2D and 3D. We start with a first-order in time SPG model. Then we show that this model needs to be modified in order to meet all the criteria we impose. Eventually, we end up with a third-order in time model. The technique is implemented as a Fortran program available from <https://github.com/gayfulin/SPG>.

2 SPG: Requirements

The user requirements are:

- The SPG should produce univariate, homogeneous and isotropic in space, and stationary in time spatio-temporal Gaussian pseudo-random fields on 3-D and 2-D spatial domains.

- The SPG should be fast enough so that it does not significantly slow down the forecast model computations.
- Variance as well as spatial and temporal length scales are to be tunable.

We also require that

- Mean-square continuity in space and time as well as sample path continuity are to be guaranteed.
- The spatio-temporal covariances should obey the “proportionality of scales” principle: larger (shorter) spatial scales should be associated with larger (shorter) temporal scales.
- The SPG *Ansatz* should be flexible enough to allow for both physical-space and spectral space solutions.

3 The proposed solution

The SPG model is selected to belong to the general class of *linear evolutionary stochastic partial differential equations* (SPDE). This choice is motivated by the flexibility of this class of spatio-temporal models (e.g. Lindgren et al., 2011). In particular, for an SPDE, it is relatively easy to introduce inhomogeneity in space and time as well as local anisotropy—either by changing coefficients of the spatial operator or by changing local properties of the driving noise. One can also produce non-Gaussian fields by making the random forcing non-Gaussian (Wallin and Bolin, 2015). Physical-space discretizations of SPDEs lead to *sparse* matrices, which give rise to fast numerical algorithms. If an SPDE has constant coefficients, then it can be efficiently solved using spatial spectral-space expansions.

In this study, we develop an SPG model that relies on an SPDE with constant coefficients, so that both physical-space and spectral-space solvers can be employed. The main technique implemented in the SPG computer program is *spectral-space* based. To facilitate the spectral-space solution, the general strategy is to define the SPG model on a standardized spatial domain. The operational pseudo-random fields are then produced by mapping the generated fields from the standardized domain to the forecast-model domain. In 3D, the standardized spatial domain is chosen to be triply periodic: the three-dimensional (3-D) unit torus. In 2D, the standardized domain is the 2-D unit torus. The 3-D and 2-D cases are distinguished by the dimensionality $d = 2$ or $d = 3$ in what follows. To simplify the presentation, the default dimensionality will be $d = 3$.

4 Tentative first-order evolutionary model for SPG

The random field in question $\xi(t, \mathbf{s})$ is a function of the time coordinate t and the space vector $\mathbf{s} := (x, y, z)$, where (x, y, z) are the three spatial coordinates. Each of the spatial coordinates belongs to the the unit circle \mathbb{S}^1 , so that \mathbf{s} is on the unit torus $\mathbb{T}^3 \equiv \mathbb{S}^1 \times \mathbb{S}^1 \times \mathbb{S}^1$ (\mathbb{T}^2 in the 2-D case).

We start with the simplest general form of a first-order in time Markov model:

$$\frac{\partial \xi(t, \mathbf{s})}{\partial t} + A \xi(t, \mathbf{s}) = \alpha(t, \mathbf{s}), \quad (1)$$

where A is the spatial linear operator to be specified and α is the 4-D driving noise postulated to be homogeneous in space and white in time.

The SPG is required to be fast, so we choose A to be a *differential* operator (because, as we noted, in this case a physical-space discretization of A gives rise to a very sparse matrix).

Further, since we wish $\xi(t, \mathbf{s})$ to be homogeneous and isotropic in space, we define A to be a polynomial of the negated spatial Laplacian:

$$A := P(-\Delta) := \sum_{j=0}^q c_j (-\Delta)^j, \quad (2)$$

where $P(x)$ is the polynomial and q its degree (a positive integer). Note that the negation the the Laplacian is convenient because $(-\Delta)$ is a non-negative definite operator.

The coefficients c_j are selected to ensure that the spatial operator $\sum c_j (-\Delta)^j$ has only positive eigen-values not close enough to 0, which can be achieved if all $c_j \geq 0$ and at least one $c_j > 0$; this guarantees *stability* of the SPG.

The model Eq.(2) appears to be too rich for the purposes of the SPG at the moment, so in what follows we employ an even more reduced (but still quite flexible) form

$$A = P(-\Delta) := \mu(1 - \lambda^2 \Delta)^q, \quad (3)$$

where μ and λ are positive real parameters.

So, we start with the following SPG equation:

$$\frac{\partial \xi(t, \mathbf{s})}{\partial t} + \mu(1 - \lambda^2 \Delta)^q \xi(t, \mathbf{s}) = \alpha(t, \mathbf{s}). \quad (4)$$

4.1 Solution of the SPG model equation in spectral space

On the torus \mathbb{T}^d , a Fourier series is an expansion in the basis functions $e^{i(\mathbf{k}, \mathbf{s})} \equiv e^{i(mx+ny+lz)}$, where the wavevector \mathbf{k} is the triple of integer wavenumbers, $\mathbf{k} := (m, n, l)$. We perform the Fourier expansion for both $\alpha(t, \mathbf{s})$ and $\xi(t, \mathbf{s})$,

$$\alpha(t, \mathbf{s}) = \sum_{\mathbf{k} \in \mathbb{Z}^d} \tilde{\alpha}_{\mathbf{k}}(t) e^{i(\mathbf{k}, \mathbf{s})}, \quad (5)$$

$$\xi(t, \mathbf{s}) = \sum_{\mathbf{k} \in \mathbb{Z}^d} \tilde{\xi}_{\mathbf{k}}(t) e^{i(\mathbf{k}, \mathbf{s})} \quad (6)$$

(where \mathbb{Z} denotes the set of integer numbers) and substitute these expansions into Eq.(4). Noting that the application of $P(-\Delta)$ to $e^{i(\mathbf{k}, \mathbf{s})}$ returns $P(\mathbf{k}^2) e^{i(\mathbf{k}, \mathbf{s})}$, recalling that $P(-\Delta)$ is defined by Eq.(3), and using orthogonality of the basis functions, we obtain that Eq.(4) decouples into the set of ordinary stochastic differential equations (OSDE, see e.g. Jazwinski (1970) or Arnold (1974)) in time:

$$\frac{d\tilde{\xi}_{\mathbf{k}}}{dt} + a_{\mathbf{k}} \tilde{\xi}_{\mathbf{k}}(t) = \tilde{\alpha}_{\mathbf{k}}(t), \quad (7)$$

where

$$a_{\mathbf{k}} := \mu(1 + \lambda^2 \mathbf{k}^2)^q. \quad (8)$$

From the postulated homogeneity of α in space, its spectral-space coefficients $\tilde{\alpha}_{\mathbf{k}}(t)$ are mutually independent. Therefore, for different wavevectors \mathbf{k} , the resulting spectral-space equations, Eqs.(7)–(8), are probabilistically completely *independent* from each other. This greatly simplifies the solution of the SPG equations because instead of handling the complicated SPDE Eq.(4) we have to solve a number of independent simple OSDEs.

Further, from the postulated whiteness of α in time, all $\tilde{\alpha}_{\mathbf{k}}(t)$ are white in time random processes (see Appendix B). So, we may write

$$\tilde{\alpha}_{\mathbf{k}}(t) = \sigma_{\mathbf{k}} \omega_{\mathbf{k}}(t), \quad (9)$$

where $\omega_{\mathbf{k}}(t)$ are independent *standard* white noises, i.e. derivatives of independent standard Wiener processes $W_{\mathbf{k}}(t)$ such that

$$\omega_{\mathbf{k}}(t) dt = dW_{\mathbf{k}}(t) \quad (10)$$

and $\sigma_{\mathbf{k}}$ are *intensities* of the white-noise processes. In space, $\sigma_{\mathbf{k}}^2$ is proportional to the spatial spectrum of the driving noise $\alpha(t, \mathbf{s})$, see Eq.(5), Eq.(9), and Appendix B. If $\sigma_{\mathbf{k}} = \text{const}$, then $\alpha(t, \mathbf{s})$ is white both in space and time, otherwise $\alpha(t, \mathbf{s})$ is a colored in space noise.

As a result, the SPG model is a series of OSDEs

$$d\tilde{\xi}_{\mathbf{k}} + \mu(1 + \lambda^2 \mathbf{k}^2)^q \tilde{\xi}_{\mathbf{k}} dt = \sigma_{\mathbf{k}} dW_{\mathbf{k}}. \quad (11)$$

For practical purposes the series is truncated, so that $\mathbf{k} \equiv (m, n, l)$ is limited: $|m| < m_{\max}$, $|n| < n_{\max}$, and $|l| < l_{\max}$, where m_{\max} , n_{\max} , and l_{\max} are the truncation limits. If not otherwise stated, all the truncation limits are the same and denoted by n_{\max} .

4.2 Stationary space-time covariance functions

4.2.1 Spectral-space statistics

Equation (11) has constant in time coefficients and so it is a Langevin equation (e.g. Arnold (1974) or Jazwinski (1970), Example 4.12), whose generic form is

$$d\eta + a\eta dt = \sigma dW, \quad (12)$$

where $\eta(t)$ is the random process in question, a and σ are constants, and $W(t)$ is the standard Wiener process. Solution to Eq.(12) is known as the Ornstein-Uhlenbeck random process, whose stationary (steady-state) temporal covariance function is

$$B_\eta(t) = \frac{\sigma^2}{2a} e^{-a|t|} \quad (13)$$

(e.g. Jazwinski, 1970, Example 4.12). From Eq.(13), it is clear that a has the meaning of the inverse temporal length scale $\tau := 1/a$.

Applying Eq.(13) to the elementary random process $\tilde{\xi}_\mathbf{k}(t)$, Eq.(11), we conclude that the stationary temporal covariance function of $\tilde{\xi}_\mathbf{k}(t)$ is

$$\mathbb{E} \tilde{\xi}_\mathbf{k}(t_0) \cdot \tilde{\xi}_\mathbf{k}(t_0 + t) = b_\mathbf{k} \cdot C_\mathbf{k}(t), \quad (14)$$

where $b_\mathbf{k}$ is the spatial spectrum:

$$b_\mathbf{k} = \frac{\sigma_\mathbf{k}^2}{2\mu(1 + \lambda^2 \mathbf{k}^2)^q} \quad (15)$$

and $C_\mathbf{k}(t)$ is the temporal correlation function for the elementary random process $\tilde{\xi}_\mathbf{k}(t)$:

$$C_\mathbf{k}(t) = e^{-\frac{|t|}{\tau_\mathbf{k}}}, \quad (16)$$

where

$$\tau_\mathbf{k} := \frac{1}{a_\mathbf{k}} = \frac{1}{\mu(1 + \lambda^2 \mathbf{k}^2)^q} \quad (17)$$

is the temporal length scale associated with the spatial wavevector \mathbf{k} .

4.2.2 Physical-space statistics

In the stationary regime (i.e. after an initial transient period has passed), Eqs.(6), (11), and (14) show that the random field $\xi(t, \mathbf{s})$ is spatio-temporally *homogeneous*, i.e. invariant under shifts in space and time:

$$\mathbb{E} \xi(t_1, \mathbf{s}_1) \overline{\xi(t_2, \mathbf{s}_2)} = B(t_2 - t_1, \mathbf{s}_2 - \mathbf{s}_1), \quad (18)$$

where

$$B(t, \mathbf{s}) := \mathbb{E} \xi(t_0, \mathbf{s}_0) \cdot \overline{\xi(t_0 + t, \mathbf{s}_0 + \mathbf{s})} = \sum_{\mathbf{k}} b_\mathbf{k} C_\mathbf{k}(t) e^{i(\mathbf{k}, \mathbf{s})}. \quad (19)$$

In particular, the spatial covariance function is

$$B(\mathbf{s}) := B(0, \mathbf{s}) = \sum_{\mathbf{k}} b_\mathbf{k} e^{i(\mathbf{k}, \mathbf{s})}. \quad (20)$$

From Eq.(20), one can see that the spatial spectrum $b_\mathbf{k}$ is the Fourier transform of the spatial covariance function $B(\mathbf{s})$.

Remark. By the spectrum (e.g. $b_\mathbf{k}$), we always mean the *modal* spectrum, i.e. the variance that is associated with a single basis function (a single wavevector \mathbf{k}); the modal spectrum is not to be confused with the variance (or energy) spectrum.

4.2.3 Spatial isotropy

Isotropy is invariance of the covariance function $B(\mathbf{s})$ under rotations. If we were in \mathbb{R}^d rather than on \mathbb{T}^d , isotropy of $B(\mathbf{s}) = B(s)$, where $s := |\mathbf{s}|$, would be equivalent to isotropy of its Fourier transform (the spectrum) $b(\mathbf{k})$, so that the latter would be dependent only on the modulus of the wavevector \mathbf{k} , i.e. the total wavenumber $k := |\mathbf{k}| = \sqrt{m^2 + n^2 + l^2}$. On the torus, spectra are discrete, i.e. m, n, l take only *integer* values, so, strictly speaking, $b(\mathbf{k})$ cannot be isotropic there. To avoid this technical difficulty, we assume that $b(\mathbf{k})$ is smooth enough, which is tantamount to the assumption that $B(\mathbf{s})$ decays on length scales much smaller than the domain's extents. With this assumption, the Fourier sum in Eq.(20) can be regarded as an integral sum and so can be approximated (for the theoretical analysis only) by the Fourier integral:

$$B(\mathbf{s}) = \sum_{\mathbf{k} \in \mathbb{Z}^d} b_{\mathbf{k}} e^{i(\mathbf{k}, \mathbf{s})} \approx \int_{\mathbb{R}^d} b(\mathbf{k}) e^{i(\mathbf{k}, \mathbf{s})} d\mathbf{k}, \quad (21)$$

where $b(\mathbf{k})$ is a smooth function of real vector argument such that $\forall \mathbf{k} \in \mathbb{Z}^d, \mathbf{b}(\mathbf{k}) = \mathbf{b}_{\mathbf{k}}$.

From Eq.(21), it is obvious that $B(\mathbf{s})$ is approximately isotropic (i.e. invariant under rotations) if $b(\mathbf{k})$ is isotropic, i.e. if $b(\mathbf{k}) = b(k)$. As it follows from Eq.(15), this is the case for the random field ξ satisfying the SPG model whenever $\sigma_{\mathbf{k}}$ is approximately isotropic: $\sigma_{\mathbf{k}} \equiv \sigma(\mathbf{k}) = \sigma(k)$.

So, to obtain approximate isotropy, we should

1. Specify an isotropic spatial intensity spectrum of the driving noise, σ_k .
2. Ensure that σ_k is smoothly varying over k , or equivalently, that the spatial length scales of $\alpha(t, \mathbf{s})$ are much less than the domain's extents.

4.3 “Proportionality of scales” implies that $q = \frac{1}{2}$

As noted above, we wish the generated field ξ to enjoy the “proportionality of scales” property (Tsyrounikov, 2001), which requires that for large k , the temporal length scale $\tau_{\mathbf{k}}$ be inversely proportional to k . From Eq.(17), this implies that

$$(1 + \lambda^2 k^2)^q \sim k \quad \text{as } k \rightarrow \infty \quad \Leftrightarrow \quad \boxed{q = \frac{1}{2}}. \quad (22)$$

Note that here and elsewhere, boxed equations are the ones that present key aspects of our final SPG model.

With $q = \frac{1}{2}$, the model's spatial operator A becomes (see Eq.(3))

$$\boxed{A = \mu(1 - \lambda^2 \Delta)^{\frac{1}{2}} \equiv \mu\sqrt{1 - \lambda^2 \Delta}}. \quad (23)$$

This is a pseudo-differential operator (e.g. Shubin, 1987) with the *symbol*

$$\boxed{a(k) := \mu\sqrt{1 + \lambda^2 k^2}}, \quad (24)$$

so that the action of the operator $A = \mu\sqrt{1 - \lambda^2\Delta}$ on the test function $\varphi(\mathbf{s})$ is defined as follows. First, we Fourier transform $\varphi(\mathbf{s})$ getting $\{\tilde{\varphi}_{\mathbf{k}}\}$. Then, for all \mathbf{k} , we multiply $\tilde{\varphi}_{\mathbf{k}}$ by the symbol $a(k)$. Finally, we perform the backward Fourier transform of $\{a(k)\tilde{\varphi}_k\}$ retrieving the result, the function $(A\varphi)(\mathbf{s})$.

Obviously, there is no problem with the above fractional negated and shifted Laplacian in spectral space (as its action on test functions is well defined, see the previous paragraph). In physical space, it appears that the pseudo-differential operator A can be approximated by a discrete-in-space operator which is a *very sparse matrix*, see Appendix C. So, in both spectral space and physical space, the resulting operator A with the fractional degree $q = \frac{1}{2}$ is numerically tractable.

The spectral-space SPG model Eq.(11) becomes

$$d\tilde{\xi}_{\mathbf{k}} + \mu\sqrt{1 + \lambda^2\mathbf{k}^2}\tilde{\xi}_{\mathbf{k}} dt = \sigma_{\mathbf{k}} dW_{\mathbf{k}}. \quad (25)$$

The resulting spatial spectrum is

$$b_k = \frac{\sigma_k^2}{2\mu\sqrt{1 + \lambda^2k^2}}. \quad (26)$$

The SPG model becomes

$$\frac{\partial \xi(t, \mathbf{s})}{\partial t} + \mu\sqrt{1 - \lambda^2\Delta} \cdot \xi(t, \mathbf{s}) = \alpha(t, \mathbf{s}). \quad (27)$$

4.4 Admissible spatial spectra

Recall that the field $\xi(t, \mathbf{s})$ is required to be mean-square continuous, which implies that its variance should be finite. In this section, we explore the spatial covariance function $B(\mathbf{s})$ of $\xi(t, \mathbf{s})$ and find conditions when $B(\mathbf{s})$ is finite, which will lead us to reformulate the basic SPG model.

4.4.1 Spatial covariance functions

From Eqs.(20) and (26), we have

$$B(\mathbf{s}) = \sum_{\mathbf{k}} b_{\mathbf{k}} e^{i(\mathbf{k}, \mathbf{s})} = \frac{1}{2\mu} \sum_{\mathbf{k}} \frac{\sigma_{\mathbf{k}}^2}{\sqrt{1 + \lambda^2\mathbf{k}^2}} e^{i(\mathbf{k}, \mathbf{s})}. \quad (28)$$

From this equation and Eq.(21) with isotropic $b(\mathbf{k}) = b(k)$ and $\sigma(\mathbf{k}) = \sigma(k)$, we have

$$B(s) \approx \int_{\mathbb{R}^d} e^{i(\mathbf{k}, \mathbf{s})} b(k) d\mathbf{k} = \frac{1}{2\mu} \int_{\mathbb{R}^d} e^{i(\mathbf{k}, \mathbf{s})} \frac{\sigma_k^2}{\sqrt{1 + \lambda^2\mathbf{k}^2}} d\mathbf{k}. \quad (29)$$

It is well known (e.g. Adler, 1981; Christakos, 2012) that in the isotropic case, the d -dimensional integral in Eq.(29) reduces to a one-dimensional integral, so that in 2D,

$$B(s)|_{2D} \approx \text{const} \cdot \int_0^\infty J_0(ks) b(k) k dk \quad (30)$$

(where J_0 is the Bessel function of the first kind) and in 3D,

$$B(s)|_{3D} \approx \text{const} \cdot \int_0^\infty \frac{\sin(ks)}{ks} b(k) k^2 dk. \quad (31)$$

Now, we find the variance $\text{Var } \xi = B(0)$ evaluating Eqs.(30) and (31) at $s = 0$. Because both $J_0(x)$ and $\frac{\sin x}{x}$ tend to 1 as $x \rightarrow 0$, we obtain approximately that

$$\text{Var } \xi|_{2D} \propto \int_0^\infty b(k) k dk \quad (32)$$

and

$$\text{Var } \xi|_{3D} \propto \int_0^\infty b(k) k^2 dk, \quad (33)$$

So, for any $d \in \{2, 3\}$ (and also for $d = 1$), we have

$$\text{Var } \xi \propto \int_0^\infty b(k) k^{d-1} dk, \quad (34)$$

Now, we use Eq.(34) to examine the validity of the SPG model.

4.4.2 Finite variance requirement

From Eqs.(26) and (34), we obtain

$$\text{Var } \xi \sim \int_0^\infty \frac{\sigma_k^2}{\sqrt{1 + \lambda^2 k^2}} k^{d-1} dk < \infty. \quad (35)$$

To check convergence of the integral in Eq.(35), we examine the $k \rightarrow \infty$ limit (where $\sqrt{1 + \lambda^2 k^2} \sim k$). As we know, the integral of this kind converges if the integrand decays faster than $\frac{1}{k^{1+\epsilon}}$ with some $\epsilon > 0$, which is the case whenever

$$\sigma_k^2 \sim \frac{1}{k^{d-1+\epsilon}}. \quad (36)$$

Equation (36) implies that the requirement that $\text{Var } \xi < \infty$ cannot be satisfied if the driving-noise spectrum σ_k^2 is constant (neither in 3D, nor in 2D, nor in 1D). This means that for the SPG model Eq.(27), the driving noise $\alpha(t, \mathbf{s})$ cannot be white in space.

4.4.3 Implications for the SPG design

As we have just seen, the SPG model Eq.(4) with white in time and space driving noise α cannot both satisfy the “proportionality of scales” property and have finite variance. So, the model Eq.(4) is to be somehow changed.

The most obvious modification is to switch from the white-in-space to a colored-in-space α . This would make the spatial spectrum σ_k^2 of the field $\alpha(t, \mathbf{s})$ non-constant so that Eq.(36) could be satisfied. However, in physical space, generation of colored (in space) noise $\alpha(t, \mathbf{s})$ can be expensive. The reason is that the spatial spectrum σ_k^2 of $\alpha(t, \mathbf{s})$ should decay for large wavenumbers (as it follows from Eq.(36)). But this kind

of spectrum *cannot*, obviously, be obtained by an application of a (cheap) *differential* operator to the white noise, as the differential operator can have only a growing symbol for large wavevectors. Consequently, we would have to resort to an expensive *integral* operator to produce $\alpha(t, \mathbf{s})$ out of the white noise $\omega(t, \mathbf{s})$.

To avoid this, we propose another technique that allows us to keep relying on the white in space forcing while resolving the infinite variance problem. The solution is to increase the temporal order of the stochastic model.

5 Higher-order in time model

5.1 Formulation

The idea is, instead of introducing an expensive *integral* operator with a decaying symbol to the *right-hand side* of the model, Eqs.(1) or (4) or (27), to introduce a *differential* operator (with a growing symbol) to the *left-hand side* of the SPG equation. The simplest way of doing so is to raise the operator $\partial/\partial t + A$, which already acts in our model on ξ in the l.h.s. of Eq.(1), to a power. This implies that the *temporal order* of the SPG model increases:

$$\left(\frac{\partial}{\partial t} + \mu\sqrt{1 - \lambda^2\Delta} \right)^p \xi(t, \mathbf{s}) = \alpha(t, \mathbf{s}), \quad (37)$$

where p is the temporal order of the modified SPG model (a positive integer) and α is white in time and, as it will be shown in the section 5.3 below, can now be made white also in space. In spectral space, the model Eq.(37) becomes, obviously,

$$\left(\frac{d}{dt} + \mu\sqrt{1 + \lambda^2 k^2} \right)^p \tilde{\xi}_{\mathbf{k}}(t) = \tilde{\alpha}_{\mathbf{k}}(t). \quad (38)$$

5.2 Stationary spectral-space statistics

For each \mathbf{k} , Eq.(38) is a p th-order in time OSDE. In Appendix D, we examine the elementary random process $\tilde{\xi}_{\mathbf{k}}(t)$ and find its stationary variance $b_{\mathbf{k}}$ and temporal correlation function $C_{\mathbf{k}}(t)$ (see Table 2 there):

$$b_{\mathbf{k}} \propto \frac{\sigma_{\mathbf{k}}^2}{\mu^{2p-1} (1 + \lambda^2 k^2)^{p-\frac{1}{2}}} \quad (39)$$

and

$$C_{\mathbf{k}}(t) = \left(1 + \frac{|t|}{\tau_{\mathbf{k}}} + r_2 \frac{|t|^2}{\tau_{\mathbf{k}}^2} + \cdots + r_{p-1} \frac{|t|^{p-1}}{\tau_{\mathbf{k}}^{p-1}} \right) e^{-\frac{|t|}{\tau_{\mathbf{k}}}}. \quad (40)$$

Here r_2, \dots, r_{p-1} are real numbers (given for $p = 1, 2, 3$ in Table 2) and $\tau_{\mathbf{k}}$ is the temporal length scale associated with the spatial wavevector \mathbf{k} :

$$\tau_{\mathbf{k}} = \frac{1}{\mu\sqrt{1 + \lambda^2 k^2}}. \quad (41)$$

Specifically, for the temporal order $p = 2$, we have

$$b_{\mathbf{k}}|_{p=2} = \frac{\sigma_{\mathbf{k}}^2}{4\mu^3(1 + \lambda^2 k^2)^{\frac{3}{2}}} \quad (42)$$

and

$$C_{\mathbf{k}}(t)|_{p=2} = \left(1 + \frac{|t|}{\tau_{\mathbf{k}}}\right) e^{-\frac{|t|}{\tau_{\mathbf{k}}}}. \quad (43)$$

For the temporal order $p = 3$, we have

$$b_{\mathbf{k}}|_{p=3} = \frac{3\sigma_{\mathbf{k}}^2}{16\mu^5(1 + \lambda^2 k^2)^{\frac{5}{2}}} \quad (44)$$

and

$$C_{\mathbf{k}}(t)|_{p=3} = \left(1 + \frac{|t|}{\tau_{\mathbf{k}}} + \frac{1}{3} \frac{|t|^2}{\tau_{\mathbf{k}}^2}\right) e^{-\frac{|t|}{\tau_{\mathbf{k}}}}. \quad (45)$$

From Eq.(41), it is seen that the “proportionality of scales” property is satisfied because $\tau_{\mathbf{k}}$ is indeed inversely proportional to k for large k .

In order to achieve the desired dependency of $\tau_{\mathbf{k}}$ not only on k (which we already have from Eq.(41)), but also on λ (the greater λ the greater should be $\tau_{\mathbf{k}}$), we parameterize μ as

$$\mu = \frac{U}{\lambda}, \quad (46)$$

where $U > 0$ is the velocity-dimensioned tuning parameter.

5.3 Finite-variance criterion

Substituting b_k from Eq.(39) into Eq.(34) yields

$$\text{Var } \xi \propto \int_0^\infty \frac{\sigma_{\mathbf{k}}^2}{(1 + \lambda^2 k^2)^{p-\frac{1}{2}}} k^{d-1} dk, \quad (47)$$

where we see that $\text{Var } \xi < \infty$ with the white (i.e. constant) driving-noise spectrum $\sigma_{\mathbf{k}}^2 = \sigma^2$ whenever

$$p > \frac{d+1}{2}. \quad (48)$$

Thus, in the higher-order-in-time model Eq.(37) we can keep relying on the white in space and time driving noise $\alpha(t, \mathbf{s})$ *provided that the temporal order is large enough*: in 2D, it is required that $p \geq 2$ whilst in 3D, we have to set up $p \geq 3$.

6 Spatio-temporal covariances for the higher-order in time SPG model

6.1 Spatial correlation functions: the Matérn class

With the constant $\sigma_{\mathbf{k}} = \sigma$, the wavenumber spectrum b_k , see Eq.(39), becomes

$$b_k \propto \frac{1}{(1 + \lambda^2 k^2)^{p-\frac{1}{2}}}. \quad (49)$$

We note that this spatial spectrum together with the constraint Eq.(48) implies that the conditions of Theorem 3.4.3 in (Adler, 1981) are satisfied, so that spatial sample paths of the random field ξ are almost surely continuous, as we required in section 2.

Moreover, the spatial fields of the resulting spatio-temporal model appear to belong to the so-called *Matérn* class of covariance functions (e.g. Stein, 1999; Guttorp and Gneiting, 2006). To see this, we denote

$$\nu := p - \frac{d+1}{2} > 0, \quad (50)$$

where positivity of the parameter ν follows from Eq.(48). Then Eq.(49) rewrites as

$$b_k \propto \frac{1}{(\lambda^{-2} + k^2)^{\nu + \frac{d}{2}}}. \quad (51)$$

Equation (51) indeed presents the spectrum of the *Matérn* family of spatial correlation functions, see e.g. Eq.(32) in Stein (1999). The respective isotropic correlation function is given by the equation that precedes Eq.(32) in (Stein, 1999) or by Eq.(1) in (Guttorp and Gneiting, 2006):

$$B(s) \propto (s/\lambda)^\nu K_\nu(s/\lambda), \quad (52)$$

where K_ν is the MacDonald function (the modified Bessel function of the second kind).

The *Matérn* family is often recommended for use in spatial analysis due to its remarkable flexibility with only two free parameters: ν and λ , see e.g. Stein (1999) and (Guttorp and Gneiting, 2006). Specifically, λ controls the spatial length scale, whereas $\nu > 0$ determines the degree of spatial smoothness (the higher ν the smoother sample paths of the spatial random field, for illustration see Appendix E).

Table 1 lists the resulting spatial correlation functions for several combinations of d and p (see Guttorp and Gneiting, 2006, for details).

Table 1: Spatial correlation functions $B(s)$ for some plausible combinations of the dimensionality d and the temporal order p

d	p	$\nu = p - \frac{d+1}{2}$	$B(s)$
2	2	$\frac{1}{2}$	$e^{-\frac{s}{\lambda}}$
2	3	$\frac{3}{2}$	$(1 + \frac{s}{\lambda}) e^{-\frac{s}{\lambda}}$
2	4	$\frac{5}{2}$	$(1 + \frac{s}{\lambda} + \frac{1}{3} (\frac{s}{\lambda})^2) e^{-\frac{s}{\lambda}}$
3	3	1	$\frac{s}{\lambda} K_1(\frac{s}{\lambda})$

For a fixed d , the larger p corresponds, according to Eq.(50) to the larger ν and so to the smoother in space field ξ . This allows us to change the degree of smoothness of the generated field by changing the temporal order of the SPG model.

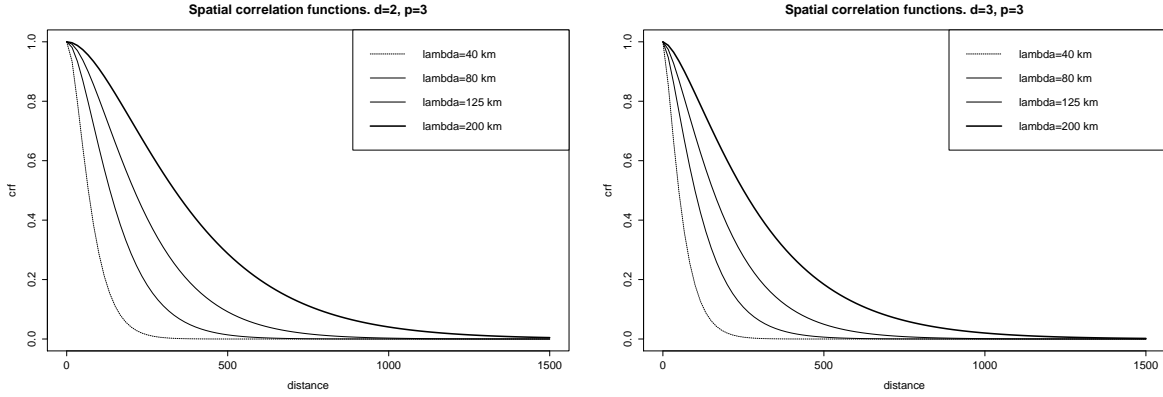


Figure 1: Spatial correlation functions for $p = 3$ in 2D (the left panel) and 3D (the right panel)—for four spatial length scales indicated in the legend.

From the constraint Eq.(48), the minimal temporal order p that can be used in both 2D and 3D is equal to 3. This value $p = 3$ will be used by default in what follows and in the current SPG computer program.

Figure 1 presents spatial correlation functions for different length scales in 2D and 3D calculated following Eq.(52). To make the plots more accessible, it is assumed here that the distance is measured in kilometers arbitrarily assuming that the extent of the standardized spatial domain (the torus) in each dimension equals 3000 km. From Fig.1, one can notice, first, that the actual length scale is indeed well controlled by the parameter λ . Second, it is seen that in 2D (the left panel), where, according to Eq.(50), $\nu = \frac{3}{2}$, the correlation functions are somewhat *smoother* at the origin than in 3D (the right panel), where $\nu = 1$. This is consistent with the above statement that the greater ν the smoother the field. But in general, the 2-D and 3-D spatial correlation functions are quite similar.

6.2 Temporal correlation functions

From Eq.(19) (which, we note, is valid for any temporal order p) evaluated at $\mathbf{s} = \mathbf{0}$, we obtain

$$B(t) = \sum_{\mathbf{k}} b_{\mathbf{k}} C_{\mathbf{k}}(t). \quad (53)$$

Here $b_{\mathbf{k}}$ is computed using Eq.(39), $C_{\mathbf{k}}(t)$ using Eq.(40), τ_k using Eq.(41), and μ is defined by Eq.(46).

Figure 2 displays the physical-space temporal correlation functions computed numerically following Eq.(53) with $U = 20$ m/s (see Eq.(46)) and $n_{max} = 90$. The left panel of Fig.2 shows $B(t)$ for the same four values of λ as in Fig.1. Again, the 2-D and 3-D correlations with the same λ are close to each other. Further, one can see that the greater λ , the greater the temporal length scale, as desired. Another important conclusion can be drawn from comparing Fig.1 and Fig.2: the *shapes* of the correlation functions in space and time are noticeably similar. This is a very nice feature because atmospheric spectra are known to be similar in the spatial and in the temporal domain, e.g. the well-known

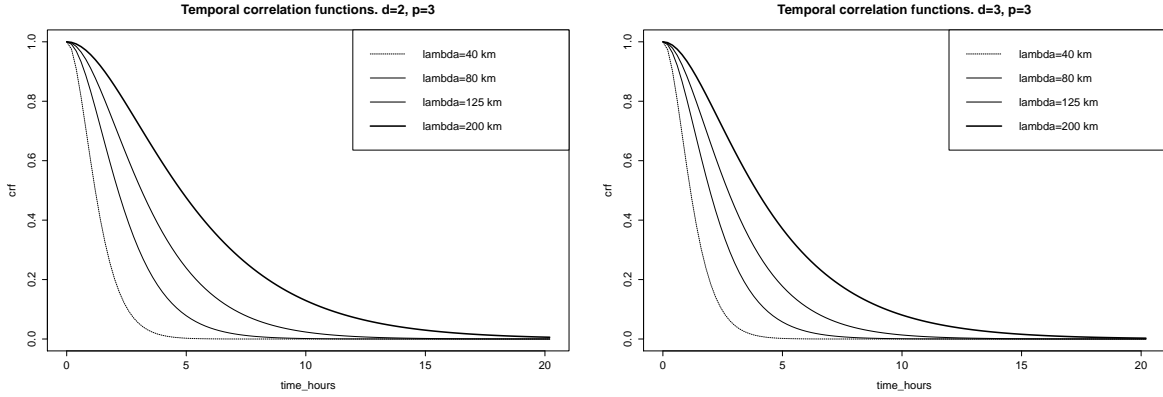


Figure 2: Same as Fig.1 but for temporal correlation functions.

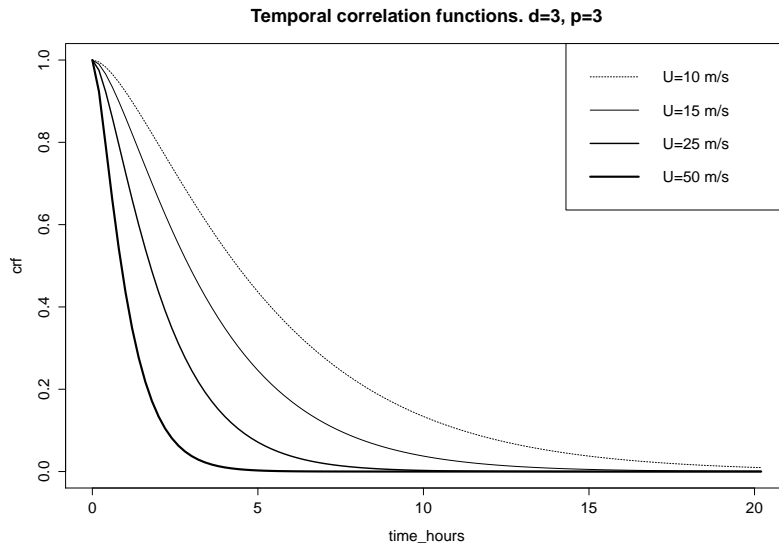


Figure 3: Temporal correlation functions in 3D for the four values of U indicated in the legend and $\lambda = 125$ km.

“-5/3” spectral slope law is observed both in space and time, see e.g. (Monin and Yaglom, 2013, section 23). So, our SPG does reproduce this observed in the nature similarity of spatial and temporal correlations.

Figure 3 shows $B(t)$ for four values of the parameter U , which controls the temporal length scale but does not affect the spatial correlations (not shown). This is in contrast to λ , which controls both the spatial and the temporal length scales, as it is seen from Figs.1 and 2.

6.3 Spatio-temporal correlations

Here, we explore 3-D spatio-temporal correlations calculated using Eq.(19) with the maximal wavenumbers in all three dimensions equal to $n_{max} = 90$, $\lambda = 125$ km, and $U = 20$ m/s. Figure 4 presents spatial correlation functions for four time lags. Figure 5 displays the spatio-temporal correlation function.

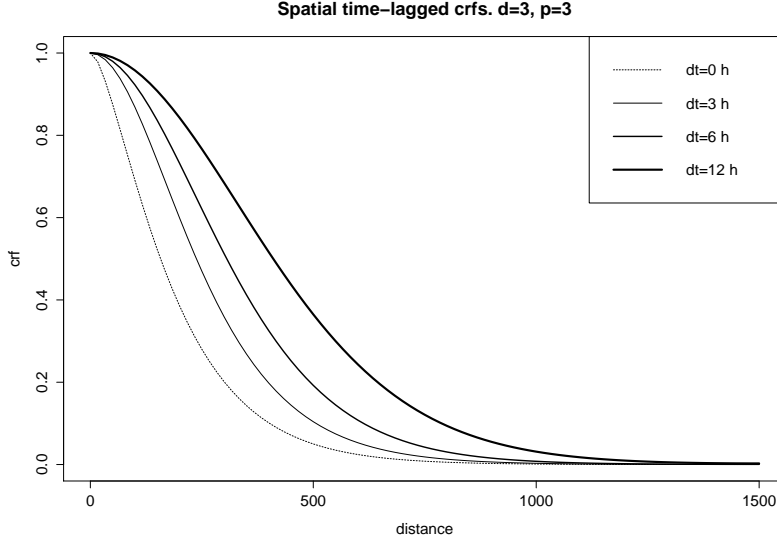


Figure 4: Spatial correlations in 3D for the four time lags indicated in the legend and $U = 20$ m/s.

From both Fig.4 and Fig.5, one can see the noticeable *non-separability* of the spatio-temporal covariances. The larger the time lag, the broader the spatial correlations. Note that this is consistent with the behavior of spatio-temporal covariances found by Cressie and Huang (1999, their Fig.8) in real-world wind speed data.

7 The final formulation of the SPG model

In the sequel, we assume that

1. The temporal order of the SPG model is $p = 3$.
2. The driving noise $\alpha(t, \mathbf{s})$ is white both in time and space, so that the intensities of the spectral-space driving noises $\tilde{\alpha}_{\mathbf{k}}(t)$ are constant: $\sigma_{\mathbf{k}} = \sigma$. The intensity of the spatio-temporal white noise α is $(2\pi)^{d/2} \sigma$.

The resulting SPG model is

$$\left(\frac{\partial}{\partial t} + \frac{U}{\lambda} \sqrt{1 - \lambda^2 \Delta} \right)^3 \xi(t, \mathbf{s}) = \alpha(t, \mathbf{s}). \quad (54)$$

In spectral space, each spectral coefficient $\tilde{\xi}_{\mathbf{k}}(t)$ satisfies the equation

$$\left(\frac{d}{dt} + \mu \sqrt{1 + \lambda^2 k^2} \right)^3 \tilde{\xi}_{\mathbf{k}}(t) = \tilde{\alpha}_{\mathbf{k}}(t) = \sigma \omega_{\mathbf{k}}(t), \quad (55)$$

where $\omega_{\mathbf{k}}(t)$ are mutually independent complex standard white noise processes.

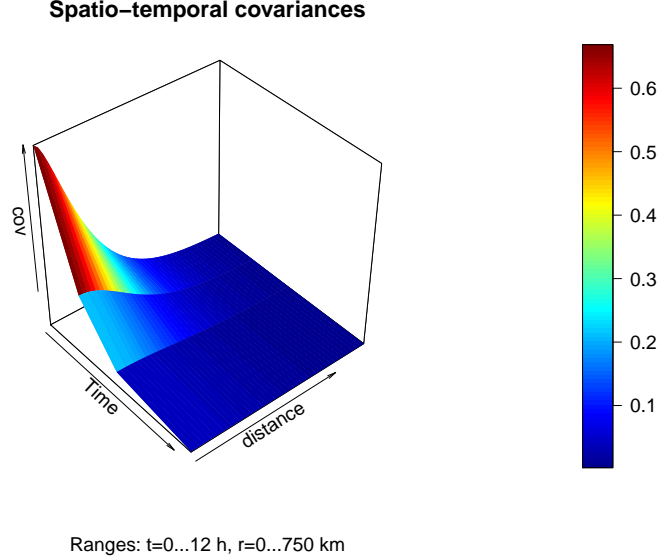


Figure 5: 3-D spatio-temporal covariances.

8 Time discrete solver for the third-order in time SPG model

In *physical space*, our final evolutionary model Eq.(54) can be discretized using the finite-difference approximation of the operator $\sqrt{1 - \lambda^2 \Delta}$ proposed in Appendix C. The respective physical-space solver looks feasible but we do *not* examine it in this study. Below, we present our basic *spectral-space* technique. From this point on, we will consider only the *spectral* SPG.

8.1 The spectral solver

To numerically integrate the SPG model equations in spectral space, we discretize Eq.(55) using an implicit scheme. The operator $(\frac{d}{dt} + a_{\mathbf{k}})^3$ (where, we recall, $a_{\mathbf{k}} := \mu\sqrt{1 + \lambda^2 k^2}$) is discretized by replacing the time derivative $\frac{d}{dt}$ with the backward finite difference $\frac{\mathcal{I} - \mathcal{B}}{\Delta t}$, where Δt is the time step, \mathcal{I} is the identity operator, and \mathcal{B} is the backshift operator. The r.h.s. of Eq.(55) (the white noise) is discretized following Appendix B, Eq.(80) with $\sigma_{\mathbf{k}} = \sigma$. As a result, we obtain the time discrete evolution equation

$$\hat{\xi}_{\mathbf{k}}(i) = \frac{1}{\varkappa^3} \left[3\varkappa^2 \hat{\xi}_{\mathbf{k}}(i-1) - 3\varkappa \hat{\xi}_{\mathbf{k}}(i-2) + \hat{\xi}_{\mathbf{k}}(i-3) + \sigma(\Delta t)^{\frac{5}{2}} \zeta_{\mathbf{k}t} \right], \quad (56)$$

where $i = 0, 1, 2, \dots$ denotes the discrete time moment, Δt the time step, $\varkappa := 1 + a_{\mathbf{k}} \Delta t$, and $\zeta_{\mathbf{k}t} \sim \mathcal{CN}(0, 1)$ are independent complex standard Gaussian pseudo-random variables (for their definition, see Appendix B.5). Note that the solution to the time discrete Eq.(56)

is denoted by the hat, $\hat{\xi}_{\mathbf{k}}(i)$, to distinguish from the solution to the time continuous Eq.(55), which is denoted by the tilde, $\tilde{\xi}_{\mathbf{k}}(t)$.

It can be shown that numerical stability of the scheme Eq.(56) is guaranteed whenever $\varkappa > 1$, which is always the case because $a_{\mathbf{k}} > 0$, see Eq.(8).

Note that the derivation of the numerical scheme for a higher-order (i.e. with $p > 3$) SPG model is straightforward: one should just raise the difference operator $\frac{\mathcal{I}-\mathcal{B}}{\Delta t}$ to a power higher than 3.

8.2 Correction of spectral variances

Because of discretization errors, the time discrete scheme Eq.(56) gives rise to steady-state spectral variances $\hat{b}_{\mathbf{k}} := \text{Var } \hat{\xi}_{\mathbf{k}}(i)$ which are different from the “theoretical” ones $b_{\mathbf{k}}$ given by Eq.(44). The idea is to correct $\hat{\xi}_{\mathbf{k}}(i)$ so that their steady-state variances coincide with $b_{\mathbf{k}}$. To this end, we derive $\hat{b}_{\mathbf{k}}$ from Eq.(56), see Eq.(95) in Appendix F, and then, knowing the “theoretical” $b_{\mathbf{k}}$, we introduce the correction coefficients, $\sqrt{b_{\mathbf{k}}/\hat{b}_{\mathbf{k}}}$, to be applied to $\hat{\xi}_{\mathbf{k}}(i)$. As a result of this correction, $\text{Var } \hat{\xi}_{\mathbf{k}}(i)$ becomes, obviously, equal to the desired spectral variances $b_{\mathbf{k}}$. This simple device ensures that the spatial spectrum and thus the *spatial* covariances are always perfect independent of the time step. But the *temporal* correlations do depend on the time step, this aspect is discussed below in section 8.4.1.

8.3 “Warm start”: ensuring stationarity from the beginning of time integration

To start the numerical integration of the third-order scheme Eq.(56) (for any wavevector \mathbf{k}), we, obviously, need three initial conditions. If the integration is the continuation of a previous run, then we just take values of $\hat{\xi}_{\mathbf{k}}(i)$ at the three last time moments i from that previous run; this ensures “continuity” of the resulting trajectory. If we start a new integration, we have to somehow generate values of $\hat{\xi}_{\mathbf{k}}(i)$ at $i = 1, 2, 3$, let us denote them here as the vector $\boldsymbol{\xi}^{ini} := (\hat{\xi}_{\mathbf{k}}(1), \hat{\xi}_{\mathbf{k}}(2), \hat{\xi}_{\mathbf{k}}(3))^{\top}$. Simplistic choices like specifying zero initial conditions give rise to a substantial initial transient period, which distorts the statistics of the generated field in the short time range.

In order to have the steady-state regime right from the beginning and thus avoid the initial transient period altogether, we simulate $\boldsymbol{\xi}^{ini}$ as a pseudo-random draw from the multivariate Gaussian distribution with zero mean and the *stationary* covariance matrix of $\hat{\xi}_{\mathbf{k}}(i)$. In Appendix F, we derive the components of this 3×3 matrix, namely, its diagonal elements V , see Eq.(95), and lag-1 and lag-2 covariances, c_1 and c_2 , respectively, see Eq.(96).

8.4 Computational efficiency

In this subsection, we describe two techniques that allow us to significantly decrease the computational cost of running the spectral SPG.

8.4.1 Making the time step Δt dependent on the spatial wavenumber k

For an ordinary differential equation, the accuracy of a finite-difference scheme depends on the time step. More precisely, it depends on the ratio of the time step Δt to the temporal length scale τ of the process in question. For high accuracy, $\frac{\Delta t}{\tau} \ll 1$ is needed.

In our problem, τ_k decays with the total wavenumber k , see Eq.(41). This implies that for higher k , smaller time steps are needed. To maintain the accuracy across the wavenumber spectrum, we choose the time step to be a certain portion of the time scale:

$$(\Delta t)_k := \gamma \tau_k. \quad (57)$$

The less γ , the more accurate and, at the same time, more time consuming the numerical integration scheme.

We note that in the atmospheric spectra, small scales have, normally, much less variance (energy) than large scales. But with the constant γ , the computational time would be, on the contrary, spent predominantly on high wavenumbers (because the latter require a smaller time step on the one hand and are much more abundant in 3D or 2D on the other hand). So, to save computer time, whilst ensuring reasonable overall (i.e. for the whole range of wavenumbers) accuracy, we specify γ to be wavenumber dependent (growing with the wavenumber) in the following simple way:

$$\gamma_k := \gamma_{min} + (\gamma_{max} - \gamma_{min}) \left(\frac{k}{k_{max}} \right)^2, \quad (58)$$

where γ_{min} and γ_{max} are tunable parameters, $k = \sqrt{m^2 + n^2 + l^2}$, and $k_{max} := \max k$.

Note that the specific values of γ depend on the definition of τ . For an OSDE of the type defined by Eq.(82) and τ defined to be equal to a^{-1} , the higher the order p , the slower the decay of the temporal correlations for the same τ . E.g. for $p = 3$ and the time lag as large as 3τ , $C(3\tau)$ appears to be as large as 0.35. In contrast, for $p = 1$, $C(3\tau) = 0.05$.

The choice of “optimal” γ_{min} and γ_{max} is discussed just below in section 8.4.2.

8.4.2 Introduction of a coarse grid in spectral space

Here we propose another technique to reduce the computational cost of the spectral solver. The technique exploits the *smoothness* of SPG spectrum b_k Eq.(44). This smoothness allows us to introduce a *coarse grid in spectral space*, perform the integration of the time discrete spectral OSDEs Eq.(56) only for those wavevectors that belong to the coarse grid, and then interpolate the spectral coefficients $\hat{\xi}_k(i)$ from the coarse grid to the full grid in spectral space.

Such an interpolation would introduce correlations between different spectral coefficients $\hat{\xi}_{\mathbf{k}}(i)$, which would destroy the spatial homogeneity. In order to avoid this, we employ a device used to generate so-called surrogate time series (Theiler et al., 1992, section 2.4.1): at each t , we multiply $\hat{\xi}_{\mathbf{k}}(i)$ by $e^{i\theta_{\mathbf{k}}}$, where $\theta_{\mathbf{k}}$ are independent *random phases*, i.e. independent for different \mathbf{k} random variables uniformly distributed on the segment $[0, 2\pi]$. It can be easily seen that this multiplication removes any correlation between the spectral coefficients.

Note also that the above random rotation of the phases does not destroy the Gaussianity because $\hat{\xi}_{\mathbf{k}}(i)$ are complex circularly-symmetric random variables with uniformly distributed and independent of $|\hat{\xi}_{\mathbf{k}}(i)|$ arguments (phases), see e.g. (Tse and Viswanath, 2005, section A.1.3).

In order to preserve the temporal correlation, we keep the set of $\theta_{\mathbf{k}}$ constant during the SPG-model time integration.

We preserve the exact spatial spectrum $b_{\mathbf{k}}$ for all \mathbf{k} after the trilinear (bilinear in 2D) interpolation of $\hat{\xi}_{\mathbf{k}}(i)$ from the coarse to the full grid as follows. At any time moment when we wish to compute the physical space field, for each \mathbf{k} on the full grid, the trilinear interpolation $\check{\xi}_{\mathbf{k}}$ is a linear combination of the closest coarse-grid points \mathbf{k}_j with $j = 1, \dots, 2^d$:

$$\check{\xi}_{\mathbf{k}} = \sum_j w_j \hat{\xi}_{\mathbf{k}_j} \quad (59)$$

where $\check{\cdot}$ denotes the interpolated value and w_j is the interpolation weight (note that the set of the closest coarse-grid points \mathbf{k}_j depends, obviously, on \mathbf{k}).

In Eq.(59), the coarse-grid variances $\text{Var } \hat{\xi}_{\mathbf{k}_j}$ are known for all \mathbf{k}_j from the spectrum $\{b_{\mathbf{k}}\}$, see Eq.(44). Therefore, we can find $\text{Var } \check{\xi}_{\mathbf{k}} = \sum_j w_j^2 b_{\mathbf{k}_j}$. Besides, we know which variance $\check{\xi}_{\mathbf{k}}$ *should* have on the fine grid, namely $b_{\mathbf{k}}$. So, we normalize $\check{\xi}_{\mathbf{k}}$ by multiplying it by $\sqrt{b_{\mathbf{k}} / (\text{Var } \check{\xi}_{\mathbf{k}})}$, thus imposing the exact spatial spectrum for all \mathbf{k} .

The 3-D coarse grid is the direct product of the three 1-D coarse grids. Any of the 1-D (non-uniform) coarse grids is specified as follows. The j th coarse grid point is located at the fine-grid wavenumber n_j , which equals j for $|j| \leq n_0$ (where n_0 is an integer) and the closest integer to $n_0(1 + \varepsilon)^{|j|-n_0}$ for $|j| > n_0$. Here, ε is a tunable small positive number.

8.4.3 Numerical acceleration: results

As the two above techniques guarantee that the *spatial* spectrum remains untouched, we test how these techniques impact the *temporal* correlations and what the speedup is.

The introduction of the coarse grid with “meaningful” parameters impacts the temporal correlations to a lesser extent than an increase in the time-step parameter γ . So, we examined the role of the two parameters of the first scheme, γ_{\min} and γ_{\max} (see section 8.4.1), and the the presence or absence of the coarse grid in spectral space.

Figure 6 shows the temporal correlations functions for different setups of the 2-D SPG indicated in the legend. The respective CPU times for the spectral-space computations

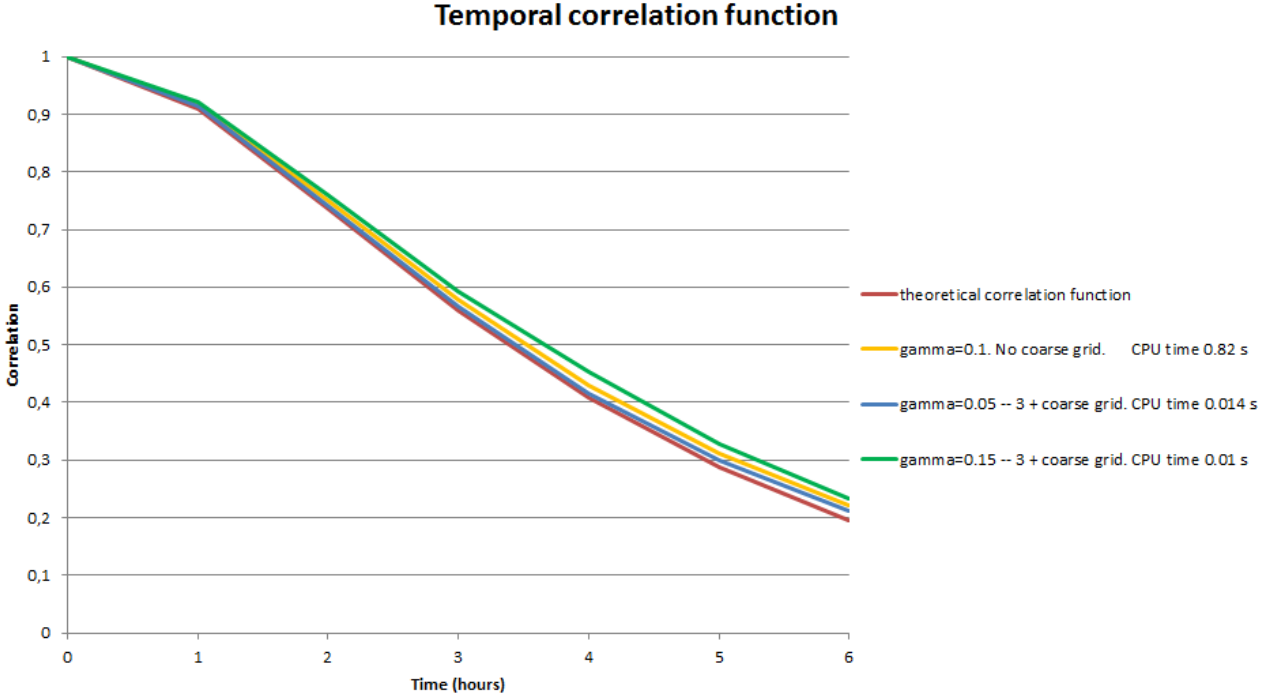


Figure 6: Theoretical and estimated temporal correlations and CPU times for a 2-D version of the SPG. The legend indicates the range $\gamma_{min} - \gamma_{max}$ and whether the coarse grid was used. The respective spectral-space computation times per one hour of SPG model time integration on one CPU are also indicated in the legend. SPG setup: $\lambda = 85$ km, $U = 12$ m/s.

(on one CPU per one hour of model integration) are also shown in the legend. The spatial model grid had 300×300 points. The coarse-grid parameters were $n_0 = 20$ and $\varepsilon = 0.2$, which resulted in the following positive coarse-grid points: 1 2 3 ... 19 20 24 29 35 42 50 60 72 86 103 124 150. The discrete backward Fourier transforms were performed every hour of the lead time.

From Fig.6, one can see that the combined effect of both numerical acceleration techniques (the green curve) was dramatic: the speedup in the 2-D scheme was about 80 times as compared to the non-accelerated scheme (i.e. without the coarse grid and with constant $\gamma = 0.1$, the yellowish curve). The contributions of the two above numerical acceleration techniques to this speedup were comparable in magnitude (not shown). Most importantly, this big speedup was achieved at a very little cost: the temporal correlation length scale was distorted, as a result of the two acceleration techniques, by only some 5 percent w.r.t. the non-accelerated scheme and some 10 percent w.r.t. the theoretical model (the red curve). Note that the speedup was for the spectral-space computations only, i.e. it does *not* include the cost of the discrete backward Fourier transform.

In summary, the 2-D SPG took only 1 second on one CPU to perform the spectral-

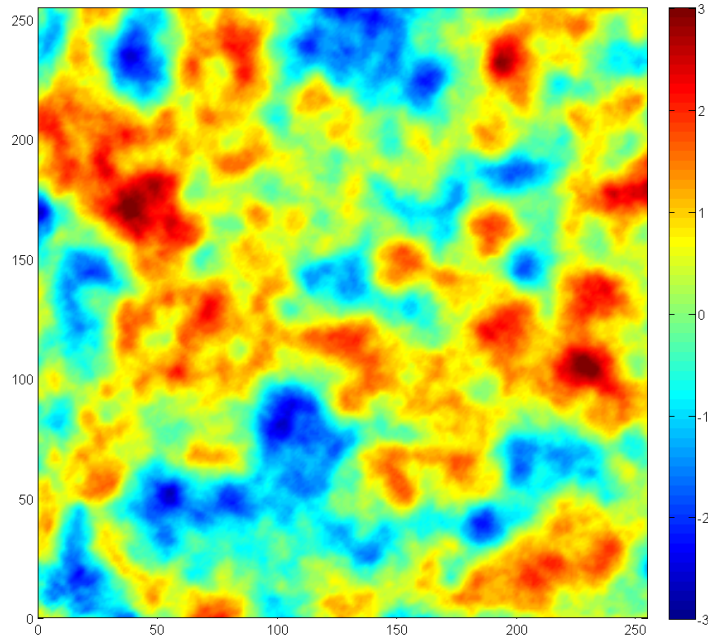


Figure 7: A 2-D (x - y) cross-section of the spatial SPG field.

space model integration for as long as 100 hours of lead time. The respective cost of the backward Fourier transform performed every hour was about 4 seconds. The total cost was thus 5 seconds.

The same computations performed for the 3-D grid with $300 \times 300 \times 64$ points took 60 seconds on one CPU for 100 hours of spectral-space model integration and 110 seconds for the backward Fourier transform. The speedup of the spectral-space computations for the 3-D scheme due to the two acceleration techniques was about 50 times.

8.5 Examples of the SPG fields

Figure 7 shows a “horizontal” cross-section and Fig.8 a spatio-temporal cross-section of a simulated pseudo-random field ξ . Note that in each spatial direction, there were 300 grid points, whilst only 256 contiguous points are shown in the Figures. This is done in the SPG for practical purposes in order to avoid correlations between the opposite edges of the spatial domain, which would be spurious in real-world applications.

9 Discussion

9.1 Physical-space or spectral-space SPG solver?

In this study, we have investigated both the spectral-space and the physical-space approximations of the SPG spatio-temporal model. We have found that both approaches can be

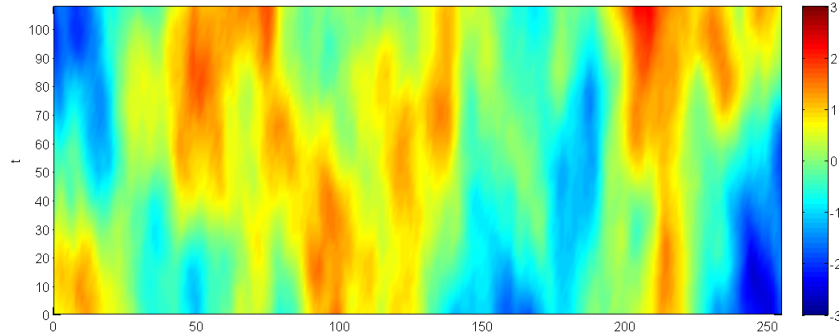


Figure 8: A 2-D (abscissa is x , ordinata is t) spatio-temporal cross-section of the SPG field.

used to build the practical SPG scheme. We have selected the spectral-space technique. Here, we briefly compare both approaches.

Advantages of the spectral-space technique are the following.

- Simplicity of realization. If the SPG model has constant coefficients, then the complicated SPG equation decouples into a series of simple OSDEs.
- Straightforward accommodation of non-local-in-physical-space spatial operators.

Advantages of the physical-space approach are:

- In physical space, it is easier to introduce inhomogeneous and anisotropic capabilities to the SPG.
- The SPG with a physical-space solver can be implemented in domains with complex boundaries.
- A physical-space solver is more suitable for an efficient implementation on massively parallel computers.

9.2 Extensions of the SPG

The proposed SPG technique can be extended in the future along the following lines.

- Development of a physical-space solver.
- Introduction of advection to the SPG model.
- Introduction of spatial/temporal inhomogeneities/anisotropy.
- Introduction of non-Gaussianity. This can be done either by applying a nonlinear transform to the output SPG fields, or by introducing a non-Gaussian driving noise (as in Wallin and Bolin, 2015). The former approach is simpler but the latter allows for much richer deviations from Gaussianity, including the multi-dimensional aspect.

- Going beyond additive and multiplicative perturbations for highly non-Gaussian variables like humidity and precipitation.
- Simulation of several mutually correlated pseudo-random fields.
- Making the temporal order p a user defined variable. As noted above, the larger p the smoother the generated field.

10 Conclusions

10.1 SPG: summary

1. The proposed Stochastic Pattern Generator (SPG) produces pseudo-random spatio-temporal fields on 2-D and 3-D spatial domains.
2. The SPG model is defined on a standardized domain in space, specifically, on the unit 2-D or 3-D torus. Fields on a limited-area geophysical domain in question are obtained by mapping from the standardized domain.
3. The SPG is based on a linear third-order in time stochastic model driven by the Gaussian white noise.
4. The spatial operator of the stochastic model is built to ensure that solutions to the SPG model, i.e. the generated pseudo-random fields satisfy the “proportionality of scales” property: large-scale (small-scale) in space field components have large (small) temporal length scales.
5. Spatial, temporal, and spatio-temporal physical-space correlations are calculated and demonstrated to possess a number of “nice” properties:
 - The spatial correlation functions belong to the Matérn class.
 - Spatial and temporal correlations have similar shapes.
 - The time-lagged spatial covariances decay slower for larger lags, as it was observed in some empirical studies.
6. It is shown that the spatial operator of the SPG model can be effectively discretized both in physical space and spectral space.
7. The basic SPG solver is spectral-space based.
8. Techniques to accelerate the spectral-space computations are proposed and implemented. The first technique selects the time step of the numerical integration scheme to be dependent on the wavenumber, so that the discretization error is smaller for more energetic spatial scales and is allowed to be larger for less energetic scales. The

second technique introduces a coarse grid in spectral space. The combined speedup for spectral-space computations from both techniques is as large as about 80 times.

9. For a brief description of the SPG, see also (Tsyrulnikov and Gayfulin, 2016).

10.2 Applications

Potential applications of the SPG include ensemble prediction and ensemble data assimilation in meteorology, oceanography, hydrology, and other areas.

The SPG can be used to generate spatio-temporal perturbations of model fields (in the additive or multiplicative or other mode), as well as boundary conditions.

Acknowledgements

The SPG has been developed as part of the Priority Project KENDA (Kilometric scale Ensemble Data Assimilation) of COSMO. We have used the discrete fast Fourier package `fft991` developed by C.Temperton at ECMWF in 1978.

Appendices

A Illustration of the “proportionality of scales” property

Figure 9 shows a realization of a spatio-temporal field with non-separable correlations that satisfy the “proportionality of scales” property (the top panel) and a realization of a field with separable spatio-temporal correlations (the bottom panel).

The non-separable spatio-temporal correlation function was defined as $B(x, t) = \exp(-r/L)$, where $r := \sqrt{x^2 + (Ut)^2}$, $U = 10$ m/s, $L = 200$ km, and the domain size in the x direction is 3000 km. The separable correlation function was $B(x, t) = \exp(-|x|/L) \cdot \exp(-|Ut|/L)$. So, both separable and non-separable fields had exactly the same spatial correlation functions and the same temporal correlation functions.

Note that both the separability and the exponential temporal correlation function is what the scale-independent first-order auto-regression used in (Li et al., 2008; Berner et al., 2009; Bowler et al., 2009; Palmer et al., 2009; Bouttier et al., 2012) yields.

Comparing the two panels of Fig.9, one can see that the two fields are quite different. In the non-separable case, Fig.9(top), large spatial structures indeed tend to live longer than small structures, as it is expected from the “proportionality of scales” principle. In contrast, in the case with separable space-time correlations, Fig.9(bottom), the “longevity” of a spatial pattern is rather independent of its size (which is unphysical). Besides, in the non-separable case, a kind of spatio-temporal “organization” is evident,

which is absent in the separable case. Finally, the field with non-separable correlations exhibits a sort of spatio-temporal isotropy, again, not visible in the separable case.

B Spatio-temporal structure of the driving 4-D noise

Here, we recall the general definition of the white noise and find its spatial spectral decomposition in the spatio-temporal case. Then we introduce a colored in space and white in time noise, and find its spatial spectrum. Finally, we define the time discrete white-noise process.

B.1 White noise

By definition, see e.g. (Rozanov, 1982, section 1.1.3) or (Kuo, 2001, section 3.1.4), the *standard white noise* $\omega(\mathbf{x})$ defined on a manifold \mathbb{D} is a *generalized random field* that acts on a test function $\varphi(\mathbf{x})$ (where $\mathbf{x} \in \mathbb{D}$) as follows:

$$(\omega, \varphi) := \int \varphi(\mathbf{x}) \Psi(d\mathbf{x}), \quad (60)$$

where Ψ is the Gaussian orthogonal stochastic measure such that for any Borel set A , $\Psi(A)$ is a (complex, in general) Gaussian random variable with $\mathbb{E} \Psi(A) = 0$ and $\mathbb{E} |\Psi(A)|^2 = |A|$, where $|\cdot|$ denotes the Lebesgue measure.

Equivalent definitions of the standard white noise are

$$\mathbb{E} |(\omega, \varphi)|^2 := \int |\varphi(\mathbf{x})|^2 d\mathbf{x}, \quad (61)$$

and

$$\mathbb{E} (\omega, \varphi) \cdot \overline{(\omega, \psi)} := \int \varphi(\mathbf{x}) \overline{\psi(\mathbf{x})} d\mathbf{x}, \quad (62)$$

where ψ is another test function. Thus, we have defined of the *standard* white noise. By the general Gaussian white noise, we mean a multiple of the *standard* white noise.

B.2 Space-integrated spatio-temporal white noise on $\mathbb{T}^d \times \mathbb{R}$

Let us consider the spatio-temporal white noise $\omega = \omega(t, \mathbf{s})$, where $t \in \mathbb{R}$ is time and $\mathbf{s} \in \mathbb{T}^d$ the spatial coordinate vector. Take a spatial test function $c(\mathbf{s})$ and define the temporal process $\Omega(t)$ formally as

$$\Omega(t) := \int_{\mathbb{T}^d} \omega(t, \mathbf{s}) c(\mathbf{s}) d\mathbf{s}, \quad (63)$$

so that it acts on a test function in the temporal domain, $\varphi(t)$, as

$$(\Omega, \varphi) := \int_{\mathbb{R}} \Omega(t) \varphi(t) dt = \int_{\mathbb{R}} \int_{\mathbb{T}^d} \omega(t, \mathbf{s}) c(\mathbf{s}) \varphi(t) d\mathbf{s} dt. \quad (64)$$

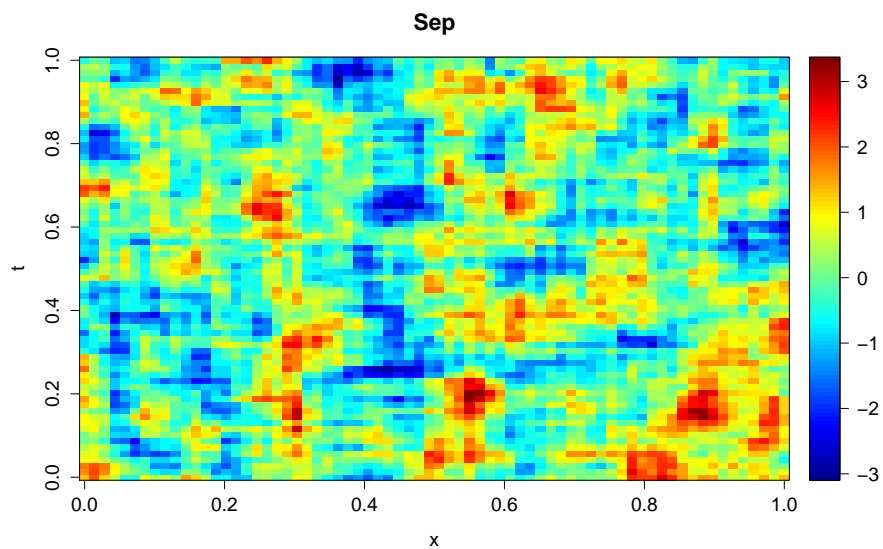
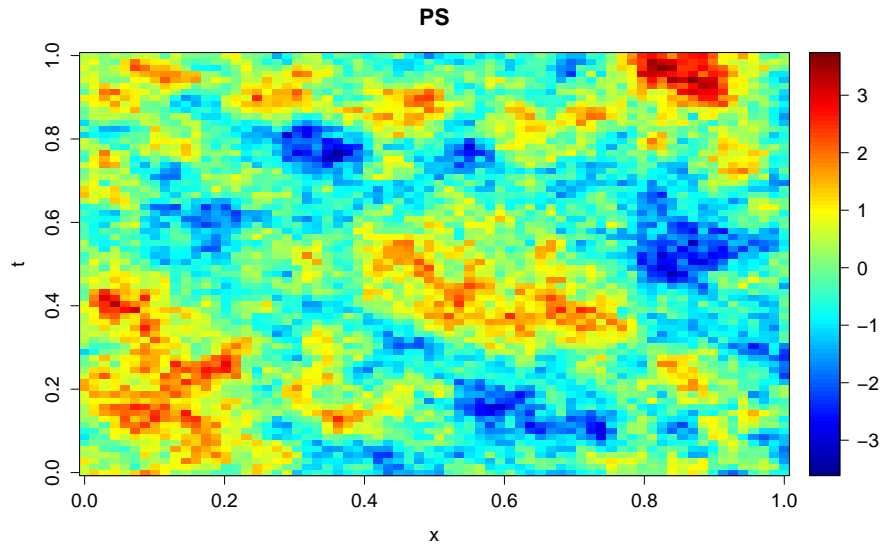


Figure 9: Simulated spatio-temporal fields. *Top*: With non-separable space-time correlations satisfying the “proportionality of scales” principle. *Bottom*: With separable space-time correlations.

Here, we note that the latter double integral is nothing other than the result of action of the original white noise $\omega(t, \mathbf{s})$ on the spatio-temporal test function $c(\mathbf{s}) \cdot \varphi(t)$. This enables us to mathematically rigorously *define* $\Omega(t)$ as the generalized random process that, with the fixed $c(\mathbf{s})$, acts on the test function $\varphi(t)$ as follows:

$$(\Omega(t), \varphi(t)) := (\omega(t, \mathbf{s}), c(\mathbf{s})\varphi(t)). \quad (65)$$

Now, using the definition of the white noise $\omega(t, \mathbf{s})$, see Eq.(61), we have

$$\mathbb{E} |(\omega(t, \mathbf{s}), c(\mathbf{s})\varphi(t))|^2 = \int_{\mathbb{T}^d} \int_{\mathbb{R}} |c(\mathbf{s})|^2 |\varphi(t)|^2 d\mathbf{s} dt = \int_{\mathbb{T}^d} |c(\mathbf{s})|^2 d\mathbf{s} \int_{\mathbb{R}} |\varphi(t)|^2 dt. \quad (66)$$

Since we have fixed $c(\mathbf{s})$, we observe that

$$\sigma^2 := \int |c(\mathbf{s})|^2 d\mathbf{s} \quad (67)$$

is a constant, such that

$$\mathbb{E} |(\Omega(t), \varphi(t))|^2 = \sigma^2 \int_{\mathbb{R}} |\varphi(t)|^2 dt. \quad (68)$$

Comparing this equation with one of the definitions of the standard white noise, Eq.(61), we recognize $\Omega(t)$ as a general Gaussian white noise in time, i.e. the standard temporal white noise multiplied by σ . We call σ the *intensity* of the white noise.

B.3 Spatial spectrum of a spatio-temporal white noise

Now, we are in a position to derive the spatial spectrum of the standard spatio-temporal white noise $\omega(t, \mathbf{s})$. In the formal Fourier decomposition

$$\omega(t, \mathbf{s}) = \sum_{\mathbf{k}} \tilde{\omega}_{\mathbf{k}}(t) e^{i(\mathbf{k}, \mathbf{s})}, \quad (69)$$

the elementary temporal processes $\tilde{\omega}_{\mathbf{k}}(t)$ can be shown to be white noises in time. Indeed, again formally, we have

$$\tilde{\omega}_{\mathbf{k}}(t) = \frac{1}{(2\pi)^d} \int_{\mathbb{T}^d} \omega(t, \mathbf{s}) e^{-i(\mathbf{k}, \mathbf{s})} d\mathbf{s}. \quad (70)$$

Here, we recognize an expression of the kind given by Eq.(63) with $c(\mathbf{s}) := e^{-i(\mathbf{k}, \mathbf{s})}/(2\pi)^d$. Therefore, from Eq.(68), $\tilde{\omega}_{\mathbf{k}}(t)$ is a temporal white noise with the intensity $\sigma_{\mathbf{k}}^{\omega}$ squared equal to

$$(\sigma_{\mathbf{k}}^{\omega})^2 = \int |c(\mathbf{s})|^2 d\mathbf{s} = \frac{1}{(2\pi)^{2d}} \int_{\mathbb{T}^d} |e^{-i(\mathbf{k}, \mathbf{s})}|^2 d\mathbf{s} = \frac{1}{(2\pi)^d}. \quad (71)$$

In addition, using Eq.(62), it is easy to show that $\tilde{\omega}_{\mathbf{k}}(t)$ and $\tilde{\omega}_{\mathbf{k}'}(t)$ are mutually orthogonal for $\mathbf{k} \neq \mathbf{k}'$.

To summarize, $\tilde{\omega}_{\mathbf{k}}(t)$ are mutually orthogonal white-in-time noises, all with equal intensities $\sigma_{\mathbf{k}}^{\omega} = (2\pi)^{-d/2}$:

$$\tilde{\omega}_{\mathbf{k}}(t) = \frac{1}{(2\pi)^{d/2}} \omega_{\mathbf{k}}(t), \quad (72)$$

where $\omega_{\mathbf{k}}(t)$ are the standard white noises.

B.4 Spectral decomposition of a white in time and colored in space noise

In order to introduce a white in time and colored in space noise, let us *convolve* the spatio-temporal white noise $\omega(t, \mathbf{s})$ with a *smoothing kernel* in space $u(\mathbf{s})$, getting

$$\alpha(t, \mathbf{s}) := \int_{\mathbb{T}^d} u(\mathbf{s} - \mathbf{r}) \omega(t, \mathbf{r}) d\mathbf{r}. \quad (73)$$

In this equation, the stochastic integral is defined, for any t and \mathbf{s} , following Eq.(65) with $c(\mathbf{r}) := u(\mathbf{s} - \mathbf{r})$. Fourier transforming $u(\mathbf{s})$,

$$u(\mathbf{s}) = \sum_{\mathbf{k}} \tilde{u}_{\mathbf{k}} e^{i(\mathbf{k}, \mathbf{s})}, \quad (74)$$

and, in space, $\alpha(t, \mathbf{s})$,

$$\alpha(t, \mathbf{s}) = \sum_{\mathbf{k}} \tilde{\alpha}_{\mathbf{k}}(t) e^{i(\mathbf{k}, \mathbf{s})}, \quad (75)$$

we easily obtain that the elementary spectral processes $\tilde{\alpha}_{\mathbf{k}}(t)$ are independent white noises in time with the intensities squared

$$\sigma_{\mathbf{k}}^2 = (2\pi)^d |\tilde{u}_{\mathbf{k}}|^2, \quad (76)$$

so that the stochastic differential $\tilde{\alpha}_{\mathbf{k}}(t) dt$ is

$$\tilde{\alpha}_{\mathbf{k}}(t) dt = \sigma_{\mathbf{k}} dW_{\mathbf{k}}(t). \quad (77)$$

Equivalently,

$$\tilde{\alpha}_{\mathbf{k}}(t) = \sigma_{\mathbf{k}} \omega_{\mathbf{k}}(t). \quad (78)$$

B.5 Discretization of the spectral processes $\tilde{\alpha}_{\mathbf{k}}(t)$ in time

Being white noises, $\tilde{\alpha}_{\mathbf{k}}(t)$ have infinite variances. They become ordinary random processes if, e.g., we discretize them in time. With the time step Δt , we define the discretized process $\hat{\alpha}_{\mathbf{k}}(t_j)$ at the time moment t_j by replacing, in Eq.(77), dt with Δt and $dW_{\mathbf{k}}$ with $\Delta W_{\mathbf{k}}$:

$$\hat{\alpha}_{\mathbf{k}}(t_j) \Delta t := \sigma_{\mathbf{k}} \Delta W_{\mathbf{k}}(t). \quad (79)$$

As $E |\Delta W_{\mathbf{k}}(t)|^2 = \Delta t$, we obtain

$$\hat{\alpha}_{\mathbf{k}}(t_j) = \frac{\sigma_{\mathbf{k}}}{\sqrt{\Delta t}} \cdot \zeta_{\mathbf{k}j}, \quad (80)$$

where $\zeta_{\mathbf{k}j}$ are independent complex standard Gaussian random variables $CN(0, 1)$. The latter is defined as a complex random variable whose real and imaginary parts are mutually uncorrelated zero-mean random variables with variances equal to $1/2$. $CN(0, 1)$ is sometimes referred to as circularly symmetric complex Gaussian (normal) random variable, see e.g. (Tse and Viswanath, 2005).

Equation (80) shows that the spatial spectrum of the time discrete driving noise is $\sigma_{\mathbf{k}}^2 / \Delta t$.

C Physical-space approximation of the operator

$$\sqrt{1 - \lambda^2 \Delta}$$

As we have discussed in section 4.3, the fractional power (square root) of the negated and shifted Laplacian operator, $\mathcal{L} := \sqrt{1 - \lambda^2 \Delta}$, is defined as the pseudo-differential operator with the symbol $\tilde{l}(\mathbf{k}) := \sqrt{1 + \lambda^2 \mathbf{k}^2}$. In the literature, one can find approaches to discretization of fractional powers of elliptic operators, see e.g. (Simpson et al., 2012), who used finite elements in the spatial context.

Here, we propose a simple technique to build a finite-difference scheme that approximates the operator $\sqrt{1 - \lambda^2 \Delta}$ in the sense that the symbol of the approximating finite-difference operator is close to $\sqrt{1 + \lambda^2 \mathbf{k}^2}$.

To this end, we do the following.

1. Perform the backward Fourier transform of the symbol $\tilde{l}(\mathbf{k})$, getting the function $l(\mathbf{s})$. As multiplication in Fourier space by $\tilde{l}(\mathbf{k})$ is equivalent to convolution in physical space with $l(\mathbf{s})$, we obtain that for any test function $\varphi(\mathbf{s})$,

$$(\mathcal{L}\varphi)(\mathbf{s}) = \int_{\mathbb{T}^3} l(\mathbf{s} - \mathbf{r}) \varphi(\mathbf{r}) d\mathbf{r}. \quad (81)$$

The crucial moment here is that the kernel function $l(\mathbf{s})$ appears to be oscillating while rapidly decreasing in modulus as $|\mathbf{s}|$ increases (see below). This enables its efficient approximation with a compact-support (truncated) function.

2. With the discretization on the grid with n points in each of d dimensions on the torus \mathbb{T}^d , the kernel function $l(\mathbf{s})$ is represented by the set of its grid-point values $l(\mathbf{s}_i)$, where $\mathbf{i} = (i_1, \dots, i_d)$ and $\mathbf{s}_i = (s_{i_1}, \dots, s_{i_d})$. If $l(\mathbf{s})$ appears to be rapidly decreasing away from $\mathbf{s} = \mathbf{0}$, we truncate the $l(\mathbf{s}_i)$ function by limiting its support near the origin, thus getting the function $l_{trunc}(\mathbf{s}_i)$. E.g. in 3D, the support of $l_{trunc}(\mathbf{s}_i)$ consists of the grid points $\mathbf{i} = (i_1, i_2, i_3)$ that simultaneously satisfy the following constraints: $|i_1| \leq J$, $|i_2| \leq J$, and $|i_3| \leq J$, where J is the spatial order of the scheme. Below, we present results with $J = 1$ (3 grid points in the support of the truncated kernel function in each dimension) and $J = 3$ (7 grid points in the support in each dimension).
3. Fourier transform $l_{trunc}(\mathbf{s})$ back to the spectral space, getting the approximated symbol $\tilde{l}_{trunc}(\mathbf{k})$.
4. Compare $\tilde{l}(\mathbf{k})$ with $\tilde{l}_{trunc}(\mathbf{k})$ and conclude whether a parsimonious (that is, with a very small J) finite-difference approximation is viable.

Now, we present the results. We found that for $d = 1$, $d = 2$, and $d = 3$, the goodness of fit was similar, so we examine the 3-D case below.

We selected the grid of $n = 2 \cdot n_{max} = 256$ points in each of the three dimensions. We specified the spatial non-dimensional length scale λ to be much greater than the mesh size

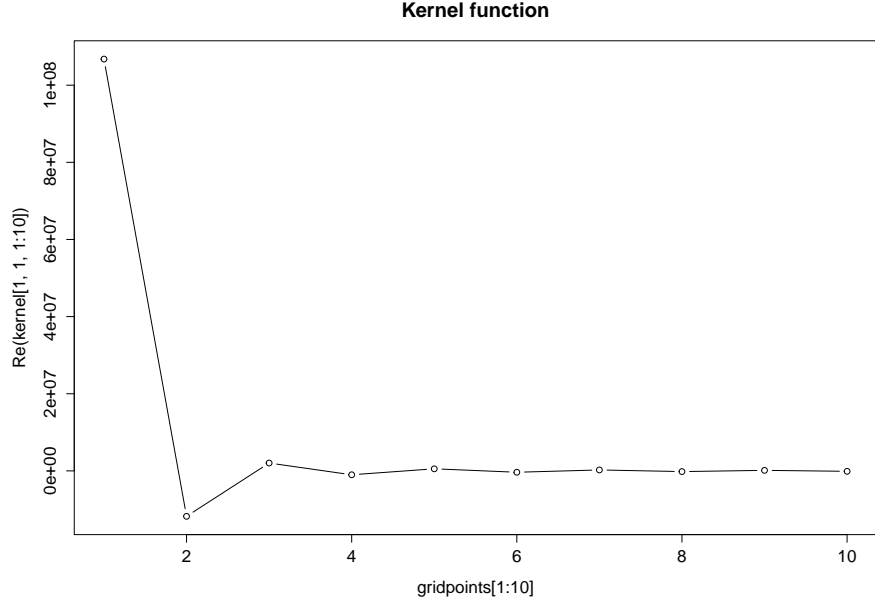


Figure 10: Kernel function

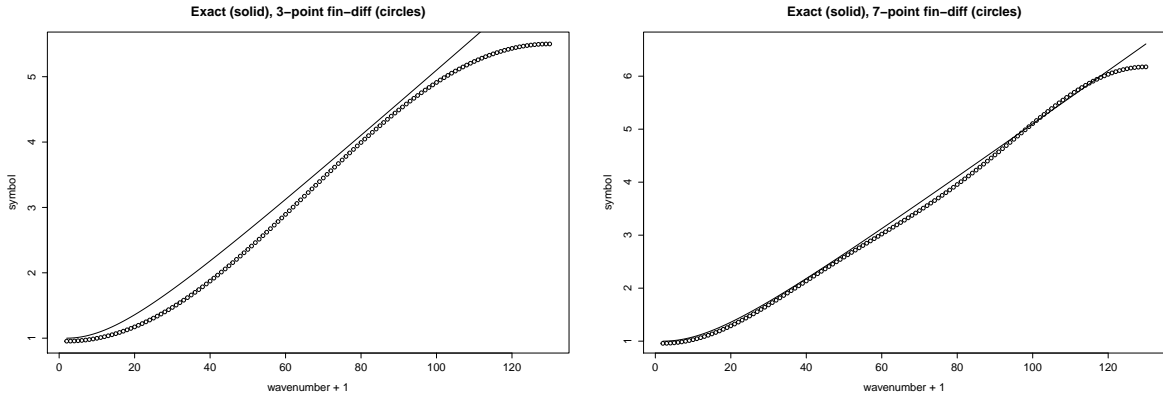


Figure 11: Goodness of fit of the symbol $\tilde{l}(\mathbf{k})$ (solid curve) by $\tilde{l}_{trunc}(\mathbf{k})$ (circles). Left: the 3-point finite-difference stencil in each dimension. Right: the 7-point stencil

$h = 2\pi/n$ and much less than the domain's extents, 2π . Specifically, we chose $\lambda = 1/n_1$, where $n_1 := \sqrt{n_{max}}$. (The results were not much sensitive to changes in n_1 within the whole wavenumber range on the grid.)

Figure 10 displays the resulting kernel function $l(s)$ for positive s (note that $l(s)$ is an even function of the scalar distance s). One can see the remarkably fast decay of $|l(s)|$ with the growing s . Consequently, a stencil with just a few points in each dimension can be expected to work well.

Figure 11 shows the exact and approximated symbols for the finite-difference stencil that contains 3 grid points in each dimension (the left panel) and the stencil that contains 7 grid points in each dimension (the right panel). (The 5-point scheme worked not much better than the 3-point one and so its performance is not shown.)

From Fig.11, one can see that the 3-point scheme's performance is rather mediocre,

whereas the 7-point scheme works very well (in terms of the reproduction of the operator's symbol).

Finally, we verified that the symbol $\tilde{l}_{trunc}(\mathbf{k})$ of the finite-difference operator for $J = 3, 5, 7$ was everywhere positive, which guarantees that the operator is positive definite and so the discretized SPG model should be stable.

To summarize, the operator $\sqrt{1 - \lambda^2 \Delta}$ can be approximated with parsimonious physical-space finite-difference schemes. For simulation of uncertainty in meteorology, where precise error statistics is rarely available, the simplest 3-point (in each direction) scheme seems most appropriate and computationally attractive. For more demanding applications, the 7-point scheme can be more appropriate.

D Stationary statistics of a higher-order OSDE

We examine the OSDE of the form Eq.(38) reproduced here without the indexes:

$$\left(\frac{d}{dt} + a \right)^p \eta(t) = \sigma \omega(t), \quad (82)$$

where σ is the real number, a is the positive number, p is the positive integer, and $\omega(t)$ is the standard white noise (see Appendix B).

The goal here is to find the variance and the correlation function of $\eta(t)$ in the stationary regime. The technique is to reduce the p -th order OSDE to a system of first-order OSDEs.

To simplify the exposition, we consider the third-order OSDE ($p = 3$) and rewrite Eq.(82) as

$$\left(\frac{d}{dt} + a \right) \left\{ \left(\frac{d}{dt} + a \right) \left[\left(\frac{d}{dt} + a \right) \eta(t) \right] \right\} = \sigma \omega(t). \quad (83)$$

Here, by η_1 we denote the term in brackets,

$$\left(\frac{d}{dt} + a \right) \eta =: \eta_1 \quad (84)$$

and by η_2 the term in braces,

$$\left(\frac{d}{dt} + a \right) \eta_1 =: \eta_2, \quad (85)$$

so that the original equation Eq.(82) can be rewritten as

$$\left(\frac{d}{dt} + a \right) \eta_2 = \sigma \omega. \quad (86)$$

In Eqs.(84)–(86), the last equation is the familiar first-order OSDE forced by the white noise, whereas the other equations are not forced by the white noise. Generalizing the above construction, Eqs.(83)–(86), to the arbitrary $p > 0$, we form the following first-order vector-matrix OSDE (a system of first-order OSDEs):

$$d\boldsymbol{\eta} + \mathbf{A}\boldsymbol{\eta}dt = \boldsymbol{\Sigma}d\boldsymbol{\omega}, \quad (87)$$

where $\boldsymbol{\eta} := (\eta, \eta_1, \dots, \eta_{p-2}, \eta_{p-1})$, $\boldsymbol{\omega} := (0, 0, \dots, 0, \omega)$, and the design of the matrices \mathbf{A} and $\boldsymbol{\Sigma}$ is obvious (not shown).

With Eq.(87) in hand, we derive a differential equation for the covariance matrix $\mathbf{P} := \mathbb{E} \boldsymbol{\eta} \boldsymbol{\eta}^*$, where $*$ denotes transpose complex conjugate (see e.g. Jazwinski, 1970, example 4.16). First, we compute the increment of \mathbf{P} :

$$\Delta \mathbf{P} = \mathbb{E} (\boldsymbol{\eta} + d\boldsymbol{\eta})(\boldsymbol{\eta} + d\boldsymbol{\eta})^* - \mathbb{E} \boldsymbol{\eta} \boldsymbol{\eta}^* = \mathbb{E} \boldsymbol{\eta} d\boldsymbol{\eta}^* + \mathbb{E} d\boldsymbol{\eta} \boldsymbol{\eta}^* + \mathbb{E} d\boldsymbol{\eta} d\boldsymbol{\eta}^*. \quad (88)$$

Then, using Eq.(87) and properties of the white noise, we obtain the differential of \mathbf{P} from Eq.(88):

$$d\mathbf{P} = -\mathbf{A}\mathbf{P}dt - \mathbf{P}\mathbf{A}^*dt + \boldsymbol{\Sigma}\boldsymbol{\Sigma}^*dt. \quad (89)$$

In the stationary regime $d\mathbf{P} = 0$, so the equation for the stationary covariance matrix is

$$\boxed{\mathbf{A}\mathbf{P} + \mathbf{P}\mathbf{A}^* = \boldsymbol{\Sigma}\boldsymbol{\Sigma}^*.} \quad (90)$$

Next, we look at the *first* diagonal entry of the resulting stationary covariance matrix \mathbf{P} , which represents the required $\text{Var } \eta$ (because η is defined above to be the first entry of the vector $\boldsymbol{\eta}$). Dropping tedious derivations, we present in Table 2 (second row) the formulas for the temporal orders $p = 1, p = 2, p = 3$, and for the general p .

Finally, we derive the temporal correlation function for the p th-order OSDE. To this end, we multiply Eq.(82) by $\eta(s)$ with $s < t$ and take expectation. Since a is non-stochastic, we may interchange the expectation and the differential operator $(\frac{d}{dt} + a)^p$, getting the p th-order ordinary differential equation for the temporal covariance function, whose solutions for different p are presented in row 3 of Table 2.

Table 2: **Variances $\text{Var } \eta$ and correlation functions $C_\eta(t)$ of the stationary solution to Eq.(82) for different temporal orders p**

p	1	2	3	Arbitrary p
$\text{Var } \eta$	$\frac{\sigma^2}{2a}$	$\frac{\sigma^2}{4a^3}$	$\frac{3\sigma^2}{16a^5}$	$\propto \frac{\sigma^2}{a^{2p-1}}$
$C_\eta(t)$	$e^{-a t }$	$(1 + a t) e^{-a t }$	$(1 + a t + \frac{a^2t^2}{3}) e^{-a t }$	$\propto R_{p-1}(a t) \cdot e^{-a t }$

Here $R_{p-1}(x)$ is a polynomial of order $p - 1$.

E Smoothness of sample paths of the spatial Matérn random field for different ν

Here, we show how sample paths (realizations) of the Matérn random field with the smoothness parameter ν look like. Specifically, in Fig.12, we present three plots with 1-D cross-sections of randomly chosen realizations of the Matérn random field for the

following three values of ν : $1/2$, $3/2$, and $5/2$. The spatial length scale parameter λ is selected in each of the three cases in such a way that the spatial correlation function intersects the 0.7 level at approximately the same distance (we denote this distance by $L_{0.7}$): $L_{0.7} = 500$ km. Again, as in section 6 and Appendix A, we assume, for convenience, that the extent of the spatial domain in each coordinate direction is 3000 km (rather than 2π). For comparison, we also display a realization with $L_{0.7} = 1500$ km for $\nu = 1/2$ (the bottom panel of Fig.12).

One can see that, indeed, the larger ν , the smoother realizations—in the sense that they have less small-scale “noise”. By contrast, increasing the length scale (compare the top and bottom panels of Fig.12) makes the large-scale pattern smoother but does *not* remove the smallest scales. So, the large-scale behavior is determined by the length scale λ , whereas the degree of smoothness/roughness on the smallest scales depends predominantly on the smoothness parameter ν .

F Stationary statistics of a time discrete higher-order OSDE

Here, to simplify the exposition, we first examine the simplest first-order (i.e. with $p = 1$) OSDE and then give the results for the third-order OSDE used in the current version of the SPG.

F.1 First-order numerical scheme

Discretization of the Langevin Eq.(12) by an implicit scheme yields

$$\eta_i - \eta_{i-1} + a\eta_i \Delta t = \sigma \Delta W_i, \quad (91)$$

so that

$$\eta_i = \frac{\eta_{i-1} + \sigma \Delta W_i}{1 + a\Delta t}. \quad (92)$$

In the stationary regime, $\text{Var } \eta_i = \text{Var } \eta_{i-1}$, whence, bearing in mind that $\text{Var } \Delta W_i = \Delta t$ and ΔW_i is independent on the values of η for all time moments up to and including the moment $i - 1$, we apply the variance operator to both sides of Eq.(92) and obtain the stationary variance

$$V(\Delta t) := \lim_{i \rightarrow \infty} \text{Var } \eta_i = \frac{\sigma^2}{2a + (g\Delta t)^2}. \quad (93)$$

Note that, as $\Delta t \rightarrow 0$, $V(\Delta t)$ tends to the continuous-time variance $\frac{\sigma^2}{2a}$, see Eq.(13).

F.2 Third-order numerical scheme

Consider the continuous-time OSDE, Eq.(82), with $p = 3$. The implicit scheme Eq.(56) we use to numerically solve it is reproduced here as

$$\eta_i = \frac{1}{\varkappa^3} [3\varkappa^2 \eta_{i-1} - 3\varkappa \eta_{i-2} + \eta_{i-3} + \sigma(\Delta t)^2 \Delta W_i], \quad (94)$$

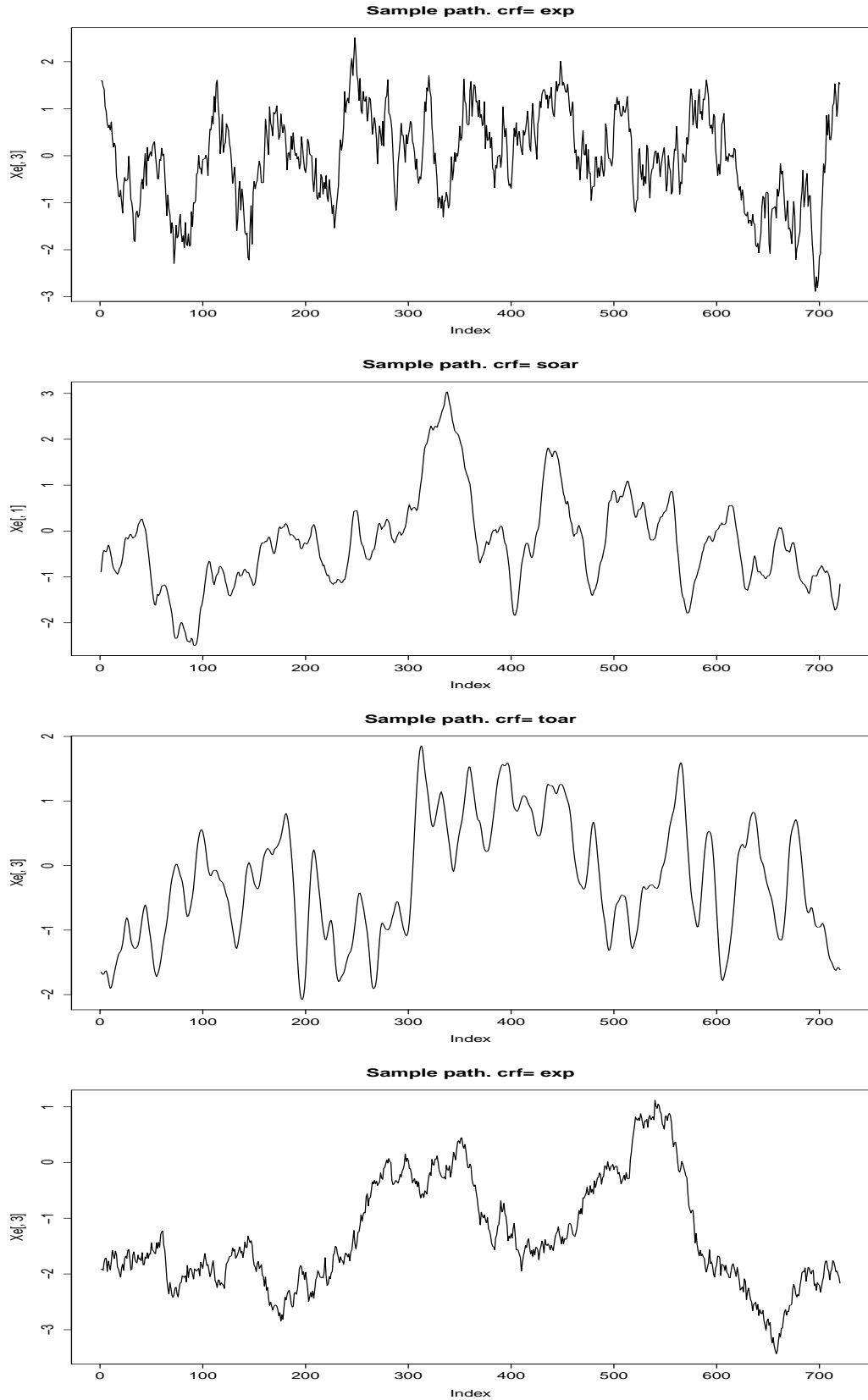


Figure 12: Sample paths for various ν and $L_{0.7}$. From the *top* to the *bottom*:
 $(\nu = \frac{1}{2}, L_{0.7} = 500), (\nu = \frac{3}{2}, L_{0.7} = 500), (\nu = \frac{5}{2}, L_{0.7} = 500), (\nu = \frac{1}{2}, L_{0.7} = 1500)$

where $\varkappa := 1 + a\Delta t$. Here, the goal is to find the stationary variance $V := \lim_{i \rightarrow \infty} \text{Var } \eta_i$ along with lag-1 and lag-2 stationary covariances, $c_1 := \lim_{i \rightarrow \infty} \mathbb{E} \eta_i \eta_{i-1}$ and $c_2 := \lim_{i \rightarrow \infty} \mathbb{E} \eta_i \eta_{i-2}$, respectively. To reach this goal, we build three linear algebraic equations for the three unknowns, V , c_1 , and c_2 . The first equation is obtained by applying the variance operator to both sides of Eq.(94). The second and third equations are obtained by multiplying Eq.(94) by η_{i-1} and η_{i-2} , respectively, and applying the expectation operator to both sides of the resulting equations.

Omitting the derivations, we write down the results:

$$V = \frac{\varkappa^4 + 4\varkappa^2 + 1}{(\varkappa^2 - 1)^5} (\Delta t)^5 \sigma^2. \quad (95)$$

$$c_1 = \frac{3\varkappa(\varkappa^2 + 1)}{(\varkappa^2 - 1)^5} (\Delta t)^5 \sigma^2, \quad c_2 = \frac{6\varkappa^2}{(\varkappa^2 - 1)^5} (\Delta t)^5 \sigma^2. \quad (96)$$

As in the first-order case, one can see that as $\Delta t \rightarrow 0$, V tends to the continuous-time variance $\frac{3}{16} \frac{\sigma^2}{a^5}$, see Table 2.

Bibliography

R. J. Adler. *The geometry of random fields*. Wiley, 1981.

L. Arnold. *Stochastic differential equations*. Wiley, 1974.

L. Bengtsson, M. Steinheimer, P. Bechtold, and J.-F. Geleyn. A stochastic parametrization for deep convection using cellular automata. *Q. J. R. Meterol. Soc.*, 139(675):1533–1543, 2013.

J. Berner, G. Shutts, M. Leutbecher, and T. Palmer. A spectral stochastic kinetic energy backscatter scheme and its impact on flow-dependent predictability in the ECMWF ensemble prediction system. *J. Atmos. Sci.*, 66(3):603–626, 2009.

J. Berner, U. Achatz, L. Batte, A. De La Camara, D. Crommelin, H. Christensen, M. Colangeli, S. Dolaptchiev, C. L. Franzke, P. Friederichs, et al. Stochastic parameterization: Towards a new view of weather and climate models. *arXiv preprint arXiv:1510.08682*, 2015.

F. Bouttier, B. Vié, O. Nuissier, and L. Raynaud. Impact of stochastic physics in a convection-permitting ensemble. *Mon. Wea. Rev.*, 140(11):3706–3721, 2012.

N. E. Bowler, A. Arribas, S. E. Beare, K. R. Mylne, and G. J. Shutts. The local ETKF and SKEB: Upgrades to the MOGREPS short-range ensemble prediction system. *Q. J. R. Meterol. Soc.*, 135(640):767–776, 2009.

R. Buizza, M. Miller, and T. Palmer. Stochastic representation of model uncertainties in the ECMWF ensemble prediction system. *Q. J. R. Meterol. Soc.*, 125(560):2887–2908, 1999.

G. Christakos. *Random field models in Earth sciences*. Courier Corp., 2012.

N. Cressie and H.-C. Huang. Classes of nonseparable, spatio-temporal stationary covariance functions. *J. Amer. Statist. Assoc.*, 94(448):1330–1339, 1999.

T. Gneiting, M. G. Genton, and P. Guttorp. Geostatistical space-time models, stationarity, separability, and full symmetry. *Monographs Statist. Appl. Probab.*, 107:151, 2006.

P. Guttorp and T. Gneiting. Studies in the history of probability and statistics XLIX. On the Matern correlation family. *Biometrika*, 93(4):989–995, 2006.

P. Houtekamer, H. L. Mitchell, and X. Deng. Model error representation in an operational ensemble Kalman filter. *Mon. Wea. Rev.*, 137(7):2126–2143, 2009.

A. Jazwinski. *Stochastic processes and filtering theory*. Academic Press, 1970.

H.-H. Kuo. White noise theory. In “*Handbook of stochastic analysis and applications*” Kannan D. and Lakshmikantham V. (Eds.), pages 107–158, 2001.

X. Li, M. Charron, L. Spacek, and G. Candille. A regional ensemble prediction system based on moist targeted singular vectors and stochastic parameter perturbations. *Mon. Wea. Rev.*, 136(2):443–462, 2008.

F. Lindgren, H. Rue, and J. Lindström. An explicit link between Gaussian fields and Gaussian Markov random fields: the stochastic partial differential equation approach. *J. Roy. Statist. Soc. B*, 73(4):423–498, 2011.

N. Meunier and J. Zhao. Observations of photospheric dynamics and magnetic fields: from large-scale to small-scale flows. *Space Sci. Rev.*, 144(1-4):127–149, 2009.

A. Monin and A. M. Yaglom. *Statistical fluid mechanics, volume II: Mechanics of turbulence*. Courier Corp., 2013.

T. Palmer, R. Buizza, F. Doblas-Reyes, T. Jung, M. Leutbecher, G. Shutts, M. Steinheimer, and A. Weisheimer. Stochastic parametrization and model uncertainty. *ECMWF Research Department Technical Memorandum n. 598, ECMWF, Shinfield Park, 42 pp.*, 2009.

Y. A. Rozanov. *Markov random fields*. Springer, 1982.

M. A. Shubin. *Pseudodifferential operators and spectral theory*. Springer, 1987.

D. Simpson, F. Lindgren, and H. Rue. Think continuous: Markovian Gaussian models in spatial statistics. *Spatial Statist.*, 1:16–29, 2012.

M. L. Stein. *Interpolation of spatial data: some theory for kriging*. Springer, New York, 1999.

M. L. Stein. Space–time covariance functions. *J. Amer. Statist. Assoc.*, 100(469):310–321, 2005.

J. Theiler, S. Eubank, A. Longtin, B. Galdrikian, and J. D. Farmer. Testing for nonlinearity in time series: the method of surrogate data. *Physica D*, 58(1-4):77–94, 1992.

D. Tse and P. Viswanath. *Fundamentals of wireless communication*. Cambridge University Press, 2005.

M. D. Tsyrulnikov. Proportionality of scales: An isotropy-like property of geophysical fields. *Q. J. R. Meterol. Soc.*, 127(578):2741–2760, 2001.

M. Tsyrulnikov and D. Gayfulin. A limited-area spatio-temporal stochastic pattern generator for ensemble prediction and ensemble data assimilation. *Meteorol. Zeitschrift (in preparation)*, 2016.

M. Tsyrulnikov and V. Gorin. Are atmospheric-model tendency errors perceivable from routine observations? *COSMO Newsletter No. 13*, pages 3–18, 2013.

M. D. Tsyrulnikov. Stochastic modelling of model errors: A simulation study. *Q. J. R. Meterol. Soc.*, 131(613):3345–3371, 2005.

J. Wallin and D. Bolin. Geostatistical modelling using non-Gaussian Matérn fields. *Scand. J. Statist.*, 42(3):872–890, 2015.